OULU 2012
D 1147

ACTA UNIVERSITATIS OULUENSIS

Jani Katisko

INTRAOPERATIVE IMAGING GUIDED DELINEATION AND LOCALIZATION OF REGIONS OF SURGICAL INTEREST

FEASIBILITY STUDY

UNIVERSITY OF OULU,
FACULTY OF MEDICINE,
INSTITUTE OF CLINICAL MEDICINE,
DEPARTMENT OF NEUROSURGERY;
INSTITUTE OF DIAGNOSTICS,
DEPARTMENT OF DIAGNOSTIC RADIOLOGY

ACTA UNIVERSITATIS OULUENSIS
D Medica 1147

JANI KATISKO

INTRAOPERATIVE IMAGING GUIDED DELINEATION AND LOCALIZATION OF REGIONS OF SURGICAL INTEREST

Feasibility study

Academic dissertation to be presented with the assent of the Faculty of Medicine of the University of Oulu for public defence in Auditorium 1 of Oulu University Hospital, on 24 February 2012, at 12 noon

UNIVERSITY OF OULU, OULU 2012

Acta Univ. Oul. D 1147, 2012

Supervised by
Professor John Koivukangas
Docent Antero Koivula

Reviewed by
Professor Juha Töyräs
Assistant Professor Riku Kivisaari

ISBN 978-951-42-9750-2 (Paperback)
ISBN 978-951-42-9751-9 (PDF)

ISSN 0355-3221 (Printed)
ISSN 1796-2234 (Online)

Cover Design
Raimo Ahonen

JUVENES PRINT
TAMPERE 2012

Katisko, Jani, Intraoperative imaging guided delineation and localization of regions of surgical interest. Feasibility study

University of Oulu, Faculty of Medicine, Institute of Clinical Medicine, Department of Neurosurgery; Institute of Diagnostics, Department of Diagnostic Radiology, P.O. Box 5000, FI-90014 University of Oulu, Finland

Acta Univ. Oul. D 1147, 2012
Oulu, Finland

Abstract

In brain surgery the operated region is often removable pathological tissue or a functional nucleus. To reach the region neurosurgeons utilize imaging and guiding methods to locate and demarcate the region of surgical interest (ROSI).

This thesis has focused on the three most common intraoperative imaging modalities used in brain surgery, namely magnetic resonance imaging (MRI), ultrasound imaging (US) and computed tomography (CT). The aim was to form practical intraoperative imaging concepts for brain tumor resections and stereotactic procedures and then to evaluate their feasibility and accuracy.

A versatile intraoperative MRI (iMRI) unit based on a 0.23 T resistive C-shaped scanner was designed, assembled and studied. The horizontally open resistive magnet enabled a staged imaging protocol with adequate image quality during neurosurgical operations while minimizing patient movement between the imaging and surgical spaces. Turning off the magnetic field eliminated the safety risks associated with operating in magnetic fringe fields.

Edema attenuation was studied to investigate the capability of inversion recovery (IR) MRI-sequences to suppress signal from edema, thereby differentiating it from resectable tumor and improving image quality in the low-field MRI unit. Use of the edema suppression IR sequence was a promising tool for image guided neurosurgery (IGS) in the context of the ROSI paradigm, but its use intraoperatively was restricted by clinical limitations.

Use of the second intraoperative imaging method, US, was studied in the intraoperative MRI environment. When these intraoperative imaging modalities, US and MRI, were interlinked together using the neuronavigation method, the localization and delineation of the region of surgical interest was more reliable.

The third intraoperative imaging method, CT with limited scanning volume, was studied in stereotactic operations where exact spatial information is the fundamental property at the cost of soft tissue contrast. The concept allowed neurosurgeons to scan the patients intraoperatively in 2D- or 3D-mode, to calculate coordinates of the specific target, to control the positioning of the applied instruments and to ensure final position of implanted objects. Thus neurosurgeons obtained valuable supplemental information of the results including the possibility to exclude hemorrhages.

Results of this thesis indicate that the use of intraoperative imaging methods with the neuronavigation should be available in sophisticated neurosurgical centers and used selectively in neurosurgical operations. Users should be familiar with the benefits and limitations of applied modalities.

Keywords: computed tomography, intraoperative imaging, magnetic resonance imaging, neuronavigation, neurosurgery, region of surgical interest, ultrasound imaging

Katisko, Jani, Leikkauksen aikaisen kuvantamisen käyttö neurokirurgisen kohdealueen rajaamisessa ja paikantamisessa - soveltuvuustutkimus.

Oulun yliopisto, Lääketieteellinen tiedekunta, Kliinisen lääketieteen laitos, Neurokirurgia;
Oulun yliopisto, Lääketieteellinen tiedekunta, Diagnostiikan laitos, Radiologia, PL 5000, 90014 Oulun yliopisto

Acta Univ. Oul. D 1147, 2012
Oulu

Tiivistelmä

Tutkimus käsittelee magneettikuvauksen (MK), ultraäänikuvauksen (UÄ) ja tietokonetomografian (TT) käyttöä aivojen neurokirurgisissa operaatioissa. Päämääränä oli muodostaa edellä mainittuja menetelmiä soveltamalla leikkauksen aikaisen kuvantamisen konsepteja, joita voidaan käyttää aivotuumoreiden poistoissa ja aivojen stereotaktisissa toimenpiteissä. Työssä on myös tutkittu konseptien käytettävyyttä ja tarkkuutta.

Leikkauksen aikaisen magneettikuvauksen tutkimiseksi suunniteltiin ja toteutettiin resistiiviseen ja avoimeen 0,23 T:n MK-laitteistoon perustuva leikkauksen aikaisen magneettikuvauksen konsepti. Horisontaalisesti avoin, resistiivinen ja matalakenttäinen MK-laitteisto mahdollisti neurokirurgisen potilaan kuvantamisen tarkoituksenmukaisella kuvanlaadulla ja kirurgisen toiminnan samassa tilassa vähäisellä potilaan siirtämisellä kuvantamis- ja operointialueen välillä. Magneettikentässä työskentelyyn liittyvät riskit voitiin minimoida sammutettavan magneettikentän avulla.

Kasvainkudoksen ympärille muodostuva aivoturvotus voi hankaloittaa leikattavan alueen paikantamista. Rajapinnan korostamiseksi selvitettiin käänteispalautukseen perustuvan MK-sekvenssin mahdollisuuksia vaimentaa aivoturvotuksesta tulevaa signaalia matalakenttäisessä magneettikuvauksessa. Aivoturvotuksen suppressointi magneettikuvista todettiin lupaavaksi työkaluksi kirurgisesti poistettavan aivokasvainalueen rajaamisessa, mutta sen käytettävyys leikkauksen aikana osoittautui rajalliseksi.

Leikkauksen aikainen ultraäänikuvaus liitettiin yhteen leikkauksen aikaisen magneettikuvauksen kanssa käyttämällä apuna neuronavigointilaitteistoa. Yhdistämällä nämä kaksi leikkauksen aikaista kuvantamismenetelmää saatiin täsmällisempää tietoa operoitavan kohteen sijainnista ja rajautumisesta.

Stereotaktisen syväaivostimulaattorin asennuksen ohjaamiseksi ja kontrolloimiseksi kehitettiin menetelmä, jossa hyödynnetään kartiokeila-TT-laitteistoa leikkauksen aikana. Menetelmä mahdollisti potilaan kuvantamisen kaksi- ja kolmiulotteisesti leikkauksen aikana. Menetelmässä ratkaistiin käytetyn kuvantamislaitteen puutteellisen kuva-alan aiheuttamat rajoitukset. Tiedon avulla voitiin määrittää tarkasti kohdetumakkeiden stereotaktiset koordinaatit, kontrolloida toimenpiteen eri vaiheissa aivoissa käytettävien instrumenttien paikka ja varmentaa aivoihin jätettävien elektrodien lopullinen sijainti. Kuvantamisen avulla kyettiin poissulkemaan leikkauksen aikana mahdollinen aivoverenvuoto.

Työn tulokset osoittavat, että leikkauksen aikainen kuvantaminen ja neuronavigointi tulisi olla käytettävissä neurokirurgisissa keskuksissa. Käytettävät menetelmät tulisi valikoida toimenpiteen mukaan ja menetelmiä soveltavien tulisi olla perehtyneitä eri modaliteettien ominaisuuksiin.

Asiasanat: kirurginen kohdealue, leikkauksen aikainen kuvantaminen, magneettikuvaus, neurokirurgia, neuronavigointi, tietokonetomografia, ultraäänikuvaus

To all those patients who need neurosurgical care

Acknowledgements

The present study was carried out at the Department of Neurosurgery, Oulu University Hospital and University of Oulu, during the years 1997–2011.

While I am very grateful to everyone who has contributed this long-standing work, I would like to express my sincere thanks to following persons in particular.

I wish to express my deepest gratitude to my supervisor, Professor John Koivukangas, M.D., Ph.D., who introduced me to the subject and provided me with a unique opportunity to work and learn life and science at the Department of Neurosurgery in Oulu. His persistent support and endless enthusiasm for medical technology and science was carrying through this study. Without his dreams and magical touch to conjure up the framework, this study would have ended before it started.

I would like to thank to my second supervisor, Chief Physicist Antero Koivula, Ph.D., who introduced me to the field of medical imaging so many years ago. His positive attitude created the foundation for a young student to investigate medical imaging.

I am sincerely thankful to Professor Juha Töyräs, Ph.D., and Assistant Professor Riku Kivisaari, M.D., Ph.D., the official reviewers of the thesis, for their constructive comments and suggestions to the manuscript.

I am warmly grateful to the entire staff at Department of Neurosurgery for their support. Especially I would like to thank my neurosurgical co-authors: Juho Tuominen, M.D., whose encouraging words in private conversations pushed me forward – not forgetting his financial contribution to my fondue in Zürich, Mikko Kauppinen, M.D., who was always open to new ideas and willing to take them into practice in functional neurosurgery, my colleague Sanna Yrjänä, Ph.D., who was always positive and pushing me forward in science, and Professor Esa Heikkinen, M.D., Ph.D., who successfully peeked into my brain and 25 years later introduced me to the field of stereotaxy and functional neurosurgery.

I owe thanks to Hagen Schiffbauer, M.D., Ph.D., who gave his valuable contributions when he worked in Oulu. I like to thank Tapani Koivukangas, M.Sc. (tech.), who helped me finalize the stereotactic phantom. I would also like to express my thanks to all the staff in the operating rooms; you all did everything possible in practice.

I am grateful to my co-authors at the Department of the Diagnostic Radiology, Risto Ojala, M.D., Ph.D., Salla-Maarit Kokkonen, M.D., Ph.D., Eero Ilkko, M.D., Ph.D., and Professor Osmo Tervonen, M.D., Ph.D., I also feel heartfelt gratitude

to radiographers Salme Meriläinen, Kyösti Palomaa and Raija Ylävaara. They were always friendly and willing to help me in my research.

I owe my thanks to all staff at Philips Medical Systems MR Technologies Finland who helped us to implement the low-field MRI operating room. Especially I wish to thank Teuvo Vaara, Ph.D., and co-author Jari Erkkilä, M.Sc., for their guidance in the field of MRI. I am also grateful to the staff at Medtronic Inc. who provided necessary training for me in the field of image guided surgery.

My wonderful friends, who inspired and believed me during this long period, deserve my warmest thanks for being there and sharing my complaints and moments of joy. I wish to thank my family and relatives, who supported me on my way.

Finally, I would like to say the most tender thanks to my sunshine, Helena, who came suddenly into my life and since then weeded all the seeds of the baobabs when I was finalizing this thesis.

The iMRI project was funded by TEKES, the Ministry of Labor, Oulu University Hospital and Philips Medical Systems MR Technologies Finland.

Oulu, January 2012 Jani Katisko

Abbreviations

2D	two-dimensional
3D	three-dimensional
AVM	anteriovenous malformation
B_0	magnetic flux density of static magnetic field
B-mode	brightness mode ultrasound imaging
CT	computed tomography
CTDI	computed tomography dose index
DBS	deep brain stimulation
EDAIR	edema attenuated inversion recovery
FE	field echo
FLAIR	fluid attenuated inversion recovery
FSE	fast spin echo
ICH	intracerebral hemorrhage
iCT	intraoperative computed tomography
IGS	image guided neurosurgery
iMRI	intraoperative magnetic resonance imaging
IOUS	intraoperative ultrasound imaging
IR	inversion recovery
ir	infrared
IT	instrument tracker
kV_p	peak kilovoltage
LIS	Leksell Index System
mAs	milliampere second
MER	microelectrode recording
mGy	milligray, unit of absorbed radiation dose
MR	magnetic resonance
MRI	magnetic resonance imaging
ms	millisecond
OR	operating room
PMMA	polymethylmethacrylate
RF	radio frequency
ROSI	region of surgical interest
SDH	subdural hematoma
STN	subthalamic nucleus
T	Tesla, unit of magnetic flux density

T_1	longitudinal relaxation time
T_2	transverse relaxation time
TCS	tool coordinate system
TE	time of echo, i.e. echo time
TI	time of inversion, i.e. inversion time
TR	time of repetition, i.e. repetition time
US	ultrasound imaging, sonography
WHO	World Health Organization

List of original articles

This thesis is based on the following articles, which are referred to in the text by their Roman numerals:

I Yrjänä S, Katisko J, Ojala R, Tervonen O & Koivukangas J (2002) Versatile intraoperative MRI in neurosurgery and radiology. Acta Neurochir (Wien) 144: 271–278.

II Katisko J, Yrjänä S, Tuominen J, Kokkonen SM, Ilkko E, Erkkilä J, Shiffbauer H & Koivukangas J (2006) Cerebral edema attenuated inversion recovery MR sequence in low magnetic field: a feasibility study. Acad Radiol 13(2): 219–228.

III Katisko J & Koivukangas J (2007) Optically neuronavigated ultrasonography in an intraoperative magnetic resonance imaging environment. Neurosurgery 60(4 Suppl 2): 373–381.

IV Katisko J, Kauppinen M, Koivukangas J & Heikkinen E (2011) Stereotactic operations using the O-ARM. Manuscript.

Contents

1 Introduction

The aim of brain surgery is to operate the brain without surgically induced trauma to healthy brain tissue: *Nil nocere suprema lex*. The operated region is often removable pathological tissue or a treatable functional target.

To reach this goal neurosurgeons utilize different imaging and guiding methods in addition to classical anatomical landmarks. Preoperative information from imaging studies has been used for the evaluation of the risks and for planning the operation. Correspondingly, intraoperative imaging has been utilized for decision making and for guiding the operation, especially to confirm the object's location and demarcation.

The most valuable steps in the development of neurosurgery have been new imaging modalities based on different physical phenomena and ways to utilize the modalities for neurosurgery: ventriculography 1920, angiography 1930, ultrasound 1950, intraoperative microscope 1960, computed tomography 1970 and magnetic resonance imaging 1980 (Alexander *et al.* 1995). Stereotaxy, surgical navigation and endoscopy have been important enabling innovations.

There are three different seeing-below-the-surface imaging modalities regularly used intraoperatively in image guided neurosurgery (IGS). These are magnetic resonance imaging (MRI), ultrasound imaging (US) and computed tomography (CT). All are based on different physical phenomena.

Magnetic resonance imaging (MRI), which is based on the interaction between magnetic moments of the nuclei of the scanned object and external magnetic fields, is the most common imaging modality for preoperative planning because of its excellent imaging properties for soft tissues. However, during surgery preoperative MR images lose their spatial accuracy due to intraoperative changes called brain shift. Furthermore, differences in magnetic susceptibility and chemical shifts can cause imaging artefacts in MRI data (Bhagwandien 1994, Schenck 1996). The effects of brain shift and image artefacts can be diminished using some other imaging or control method intraoperatively. Intraoperative MRI (iMRI) has been shown to be a feasible method to control and update preoperative MRI data (Alexander *et al.* 1995a, Tronnier *et al.* 1997, Schenck *et al.* 1995, Jolesz & Blumenfeld 1994).

Computed tomography (CT) is based on ionizing x-rays and the physical attenuation of the x-rays travelling through the scanned object. Use of CT images for planning and guiding neurosurgical operations is more sparse than the use of MR images, but CT can be used to ensure spatial accuracy of the MRI images

(Alexander *et al.* 1995b). CT is the primary scanning method for patients with contraindications for MRI scanning, e.g. patients with cardiac pacemakers or deep brain stimulators. It is also commonly used for stereotactic operations to calculate target coordinates.

Ultrasound imaging (US) is based on mechanical waves which are scattered back from the surfaces or interfaces inside the scanned object. Despite limitations of interpretation in the US images, the method holds an important role in neurosurgery as an intraoperative imaging method. Intraoperative changes can be checked fast and easily with US.

In addition to the above mentioned three different scanning methods – MRI, CT and US – other imaging modalities are also utilized for image guided neurosurgery, such as PET (positron emission tomography) (Bittar *et al.* 1999, Braun *et al.* 2001), SPECT (single photon emission computed tomography) (Hogan *et al.* 1999), MSI (magnetic source imaging) (Ganslandt *et al.* 1997), MRA (magnetic resonance angiography) (Hall *et al.* 2003), MRS (magnetic resonance spectroscopy) (Son *et al.* 2001, Hall *et al.* 2003), fMRI (functional magnetic resonance imaging) (Roux *et al.* 2001, Braun *et al.* 2001), DTI (diffusion tensor imaging) (Talos *et al.* 2003), TMS (transcranial magnetic stimulation) (Krings *et al.* 1997) and optical imaging (Stummer *et al.* 1998).

Image datasets obtained from different imaging modalities are exploited for image guidance via computer aided systems called neuronavigators. With the neuronavigator the imaged patient and the obtained image dataset can be co-registered and the image dataset can be visualized to show the position and direction of an instrument during surgery. Thus, the operated region can be visualized and the region of surgical interest (Koivukangas *et al.* 2003) can be located, characterized and demarcated using an appropriate localization method.

The aim of this doctoral thesis was to form practical intraoperative imaging concepts for brain tumor resections and stereotactic procedures and to evaluate the feasibility and accuracy of the concepts. All four studies in this thesis were designed to clarify the value of intraoperative imaging methods for visualizing surgical areas in different operations and to investigate whether fusion of the different imaging modalities based on various physical phenomena could help neurosurgeons to analyze the region of surgical interest.

2 Review of the literature

2.1 The physics behind the imaging methods used

All imaging modalities can be simplified by using a black box model where an unknown object can be studied by feeding a known input into the stable system, causing an unstable situation, and then measuring how the system returns back to equilibrium. In the returning phase, the system sends energy, which is the system's output. The image can be constructed based on the relationship between input and output. In most medical imaging methods the applied input is radiation energy. In ultrasound imaging the applied energy is mechanical sound waves of ultrasonic wavelengths. In MRI the used energy is electromagnetic waves in the radiofrequency band. In CT the utilized energy is also electromagnetic waves, x-rays that have far shorter wavelengths than are used in MRI. The used form of energy interacts with the scanned object in a way that is characteristic of its physical properties. The physical properties of the radiation influence how the scanned object interacts with and responds to the stimulus.

MRI, magnetic resonance imaging, is based on the interaction between the magnetic moments of the nuclei of the scanned object and the external magnetic fields. Nuclei should have nonzero spin, which can be taught to possess the magnetic moment of nuclei. In neurosurgical applications the imaged nuclei are usually those of hydrogen atoms, i.e. protons. The human body consists largely of water and each water molecule includes two hydrogen nuclei or protons. During scanning, a strong static and homogeneous B_0 magnetic field (usually 0.12–3.0 T) aligns all nuclei with nonzero spin to rotate around the B_0 field at the Larmor frequency (^{1}H: 42.58 MHz/T). A proton has two energy levels where it can align itself – low and high energy levels. According to Boltzmann's statistic there is a very small difference between low and high energy level orientated spins. This difference is caused in stable net magnetization which can then be manipulated and measured. By feeding electromagnetic energy at the Larmor frequency into the scanned object, the net magnetization in the stable state can be driven into an unstable state. While absorbing energy, spins at a low energy level go over to a higher level turning the orientation of the net magnetization. After energy feeding is stopped the system starts to stabilize itself and the spins return to the stable state, sending measurable energy outside the object. MR images are constructed from these radio frequency signals sent by hydrogen atoms when returning from

the unstable state. To obtain spatial information, the static magnetic field is changed with gradient fields which cause mild changes in the Larmor frequencies. The contrast in MR images results mainly from the variations of the density of hydrogen atoms in different tissues. Variations of signal intensity are influenced by four factors; proton density, relaxation times T_1 and T_2 and the flow intensity of the protons (Smith & Ranallo 1989).

MRI is based on static and changing electromagnetic fields, which should be taken into account when operating inside the scanning volume or at a close vicinity to the scanner in the fringe fields. This places special requirements on applied instruments and equipment. Depending on how close to the magnetic field instruments or equipment are used, they have to fulfil safety requirements and thus be classified as either MRI-safe or MRI-compatible.

Computed tomography (CT) is based on x-rays and the physical attenuation of the x-rays in the scanned object. The contrast in the CT images depends on the attenuation differences of tissues, thus depending on only two parameters: electron density in the tissue and the effective atomic number (Judy 1995). CT images are less often used for planning and guiding neurosurgical operations than MR images, but CT could be used to ensure and correct the spatial accuracy of the MRI images (Alexander *et al.* 1995b). CT is the primary scanning method for those patients with limitations regarding MRI scanning, e.g. patients with cardiac pacemakers or deep brain stimulators. CT is commonly used for stereotactic operations to calculate target coordinates. This thesis shows how a CT-like 3D scanning system, the O-arm, could be applied also in stereotactic operations.

Ultrasound imaging (US) is based on mechanical waves which travel through the scanned object. Mechanical waves reflect from and/or are scattered partially by the boundaries of tissues with differing acoustic impedances. The returning acoustic waves can be detected by the US transducer and are used for image formation when the speed of the mechanical waves is known. (Wells 1978b, Kiuru 1985). Despite obscure areas in US images, US has an important role in neurosurgery as an intraoperative imaging method. Intraoperative changes can be checked quickly and easily with an US system.

2.2 Ultrasound imaging in neurosurgery

2.2.1 History of ultrasound imaging in neurosurgery

The use of ultrasound has been developed since 1880, when Pierre and Jacques Curie discovered that quartz crystals formed a potential effect from mechanical stimuli. They also argued the opposite reaction, that an electronic stimulus induced a change in crystal dimensions. It was not until forty years later, in 1920, that ultrasound was presented as a new type of radiation travelling in a biological medium and it was then that the medical possibilities of ultrasound were understood. Düssik (1942) used ultrasound transmission technique to produce the first US image of the brain. This was followed by rapid development of ultrasound as a therapy and imaging method. (Hill 1973, Wells 1978a). The use of ultrasound became even more common in 1955 when Jaffe *et al.* found piezoelectricity in lead zirconate titanate (PZT) (Wells 1978a), which is widely used today.

In neurosurgery ultrasound has been used since 1944, when Lynn and Putnam were trying to cause brain injuries in 3 dogs, 30 cats and 4 monkeys using 1 MHz focused ultrasound. They forgot to take into account the attenuation of ultrasound in the skull bone. The first therapeutic neurosurgical application was a method presented by Lindstrom in 1954 in which ultrasound applied through a skull opening substituted the lobotomy operation (Lindstrom 1954). The actual use of ultrasound as a neurosurgical imaging method was started in 1950 when French and others investigated intracranial pathologies using the United States Navy 15 MHz transducer (French *et al.* 1950, French *et al.* 1951). Also, Wild and Reid, in 1953, showed ultrasound echo differences obtained from normal and abnormal brain tissues (Wild & Reid 1953). In 1955, Leksell introduced echoencephalography for the determination of the brain midline (Leksell 1956). The shifted midline was assumed to be a marker for existing intracranial pathologies. The method was widely used until the introduction of CT (Redfern 1993).

2.2.2 Ultrasound as an intraoperative imaging method

Real-time ultrasound imaging in B-mode (B, brightness) has been used intraoperatively since the early 1980s. The technique was developed independently of each other at four locations simultaneously (Chandler & Rubin

1986) and has been routinely used since 1981 at the Department of Neurosurgery, Oulu University Hospital. By 1985, ultrasound imaging was used intraoperatively to locate subcortical brain tumors and to search for remnants of a tumor. In addition, ultrasound was used to locate hematomas, vein abnormalities, infections, abscesses and cysts inside the tumors.

Real-time B-mode ultrasound was also used for guiding brain biopsies. Yamasaki *et al.* have described the use of the Doppler technique during stereotactic biopsy of malignant tumors (Yamasaki *et al.* 1994). At that time Mayfrank *et al.* reported on how to use ultrasound imaging guidance for craniotomy (Mayfrank *et al.* 1994). They scanned the brain using an ultrasound probe through a trepanation of 12 mm and were able to determine the place of the craniotomy more accurately and to avoid an unnecessarily large opening. A Norwegian research team led by Gronningsaeter was probably the first to report on the use of catheter ultrasound probes (Gronningsaeter *et al.* 1996). The group applied the probes intended for intravascular imaging in cardiology. High-frequency catheter probes could be placed in a saline-filled resection cavity. High resolution and a short distance to boundaries of the region of surgical interest helped to control the progression of the operations.

3D ultrasound imaging has also been studied (Koivukangas 1984, Kavic 1995, Kossoff *et al.* 1995, Fenster & Downey 1996). The most advanced in the field of three-dimensional ultrasound imaging is Gronningsaeter's group. They have made a commercial navigation system which uses navigation to collect the 3D ultrasound image data. The obtained 3D image data can then be navigated at the same time with the corresponding preoperative MR imaging data (Gronningsaeter *et al.* 2000, Unsgaard *et al.* 2002, Unsgaard *et al.* 2006).

2.2.3 Clinical impact of intraoperative ultrasound imaging

Intraoperative real-time ultrasound has been used successfully for imaging intracranial tumors since 1980 (Voorhies & Patterson 1980, Masuzawa *et al.* 1981, Chandler *et al.* 1982, Grode & Komaiko 1983, Koivukangas 1984, Rubin & Dohrmann 1985, Knake *et al.* 1985, Quencer & Montalvo 1986, Sutcliffe 1991). It has been shown that ultrasound imaging is an effective method in many situations, such as locating tumors, cysts and necrosis, defining borders and guiding the surgeon to the target and identifying possible tumor remnants (Rubin & Dohrmann 1983, Rubin & Dohrmann 1985, Sutcliffe 1991, Rubin & Chandler 1990, Gooding *et al.* 1983). In many cases, ultrasound localization is a crucial

task, because it provides certainty and speeds up the operations (Hammoud *et al.* 1996). Common use of US is based on the simplicity of the systems and economical aspects compared to other intraoperative methods. The equipment used varies from simple handheld B-mode scanners to systems with multifunctional properties, such as 3D-imaging, Doppler and tools for measurement. State-of-the-art ultrasound units are 3D-scanning systems with navigation possibilities.

The literature indicates growing evidence of the clinical impact of gross-total macroscopic resection of gliomas on recurrent growth and patient survival (McGirt *et al.* 2009, Sanai & Berger 2008, Stummer *et al.* 2006). However, among a number of feasibility studies, there are no clinical studies showing increased survival or better quality of life after intraoperative US guided surgery (Jakola *et al.* 2011).

2.3 Magnetic resonance imaging in neurosurgery

Features of magnetic resonance imaging – excellent soft tissue contrast, opportunity to have 3D images in whichever slice direction and the lack of ionizing radiation – have promoted the use of MRI as a neurosurgical imaging method. The sensitivity of the method to interference and the risk factors due to static and alternating magnetic fields have, however, limited use of MRI only to suitable scanning rooms. Therefore, the patient's imaging is usually done preoperatively.

During surgery brain tissue shifts because of leaking cerebrospinal fluid. In tumor resections, removal of the tumor tissue also causes shifts. Therefore, the real intraoperative anatomy may differ from the anatomy in preoperative images. Thus, it has been found necessary to develop the use of intraoperative MRI.

2.3.1 History of magnetic resonance imaging in neurosurgery

Nearly four decades after the publication of nuclear magnetic resonance (Bloch *et al.* 1946, Purcell *et al.* 1946), magnetic resonance imaging was used for imaging of the brain. MRI scanning of physiologically minimally moving targets, such as the brain, was possible thanks to the Fourier transform and the NMR (nuclear magnetic resonance) imaging method which were based on linear magnetic field gradients and the method of projection reconstruction published by Lauterbur (Lauterbur 1973).

The first brain imaging was done in the beginning of the 1980s. Carr *et al.*'s study into the use of contrast agents for imaging brain of lesions in 1984, Masaryk *et al.*'s article on brain MR angiography in 1989, Ogawan *et al.*'s 1990 and Belliveau *et al.*'s 1990 studies on functional magnetic resonance imaging and Moseley *et al.*'s 1990 article on diffusion imaging have been essential stages in the development of MRI to become the standard neurosurgical imaging method. (Redpath 1997)

2.3.2 Magnetic resonance as an intraoperative imaging method

Jolesz and Blumenfeld presented in 1994 a wide range of applications, as to how MRI was thought to be exploited to guide and control the various mini-invasive treatments (Jolesz & Blumenfeld 1994). Even before that, in 1988, General Electric had launched a project whose goal was to create an MRI scanner allowing intraoperative magnetic resonance imaging (iMRI) (Jolesz 1994). However, Heidelberg's group performed the first brain tumor operation with iMRI in May 1996 (Wirtz *et al.* 1997). It was one month earlier than the first iMRI guided brain operation in Boston (Black *et al.* 1997).

Several different neurosurgical iMRI concepts have been presented since 1995. Concepts vary widely depending on the used scanners, the practices employed to combine imaging as well as surgical environment and the methods of navigation. The concepts may be divided to groups according to the magnetic field strength of the scanner: low-field ($B < 0.5$ T), mid-field ($0.5 \leq B < 1.5$ T) and high-field ($B \geq 1.5$ T) systems.

Low-field scanners, B < 0.5 T

The low-field MRI scanners have been widely applied intraoperatively due to their open structure.

The two-room concept, based on a separate scanning room and an immediate vicinity located operating room (OR), was first proposed from the Heidelberg University Hospital in Germany. Surgical operations were carried out in the operating room, from where the patient was transported to the scanning room using a mobile operating table (Tronnier *et al.* 1997, Wirtz *et al.* 1997).

The Erlangen group reported on using a concept similar to that of Heidelberg in 1998, in which patients were transferred between the scanning and operating rooms (Steinmeier *et al.* 1998). Later, however, they ended up operating in the

scanning room outside the 0.5 mT safety boundary (Nimsky *et al.* 2001), which allowed the use of conventional non-MRI compatible tools and a surgical navigation microscope.

The solution at the University of Cincinnati was also based on a combination of separate scanning and operating rooms. A clear distinction to the previously published concept was the use of scanning equipment for diagnostic imaging of patients outside the operating room. (Bohinski *et al.* 2001)

In Toronto a custom-made prototype of a 0.2 T scanner based on permanent static magnets was used. The patient was transferred along the longitudinal axis between the scanning and operating areas. Almost all the conventional surgical instruments could be used when the patient was moved more than one meter from the scanner. (Bernstein *et al.* 2000)

At the University of California in Los Angeles a horizontally open, 0.2 T resistive MRI unit was used. A similar scanner was applied also in Heidelberg's and Erlangen's concepts. Their operating and scanning table could be rotated. Thus, the patient on the rotatable table could be turned between the imaging and operating area without changing the patient's surgical position significantly. During surgery the patient was translated to the area where the fringe magnetic fields do not affect the use of ordinary surgical instruments and tools. (Rubino *et al.* 2000)

In Tel Aviv (Hadani *et al.* 2001) and in Brussels (Levivier *et al.* 2003) an iMRI scanner has been used that was designed exclusively for neurosurgery. The concept consists of a 0.12 T scanner called PoleStar and an optical navigation device. During surgical operations the scanner is placed under the operating table. When images are needed, the two permanent magnetic poles are raised to the operating area. The surgeon's working space is adequate during the imaging period. Unlike Hadani's concept based on a radio frequency (RF) shielded room, Levivier used a mobile "RF-tent", which was pulled around the patient while scanning in order to shield the area. After Hadani and Levivier, the PoleStar has been used widely, and is the most implemented iMRI scanner in the world.

The Oulu concept of iMRI was routinely used for brain tumor resections since 1999. This versatile concept was based on a C-shaped resistive magnet and optical navigation system. The Oulu concept was designed for combined neurosurgical, interventional and diagnostic use.

Mid-field scanners, 0.5 ≤ B < 1.5 T

The first complete iMRI concept was introduced in 1995 at Boston's Brigham and Women's Hospital (Schenck *et al.* 1995, Alexander *et al.* 1995b). This mid-field double donut 0.5 T scanner was based on two vertically parallel superconducting coils. The surgeon worked between the vertical coils in the 56 cm wide gap, where the patient had been transferred through the 55 cm wide holes in the centers of the coils. The navigation method used active optical localization. This concept was applied in many centers (Black *et al.* 1997, Kollias *et al.* 1998, Samset & Hirschberg 1999, Seifert *et al.* 1999, Tyler & Mandybur 1999).

High-field scanners, B ≥ 1.5 T

The University of Calgary reported on using a roof-rails movable 1.5 Tesla scanner (Sutherland *et al.* 1999). Later, Kaibara *et al.* published the original concept, stating that it had to be modified significantly (Kaibara *et al.* 2000). The idea in the concept was to transport the on-rails-hanging scanner to the operating room for the imaging session. At that time, the non-MRI-compatible and -safe instruments and equipment were moved outside the security boundary. Between imaging sessions the scanner was placed in a storage room at close vicinity. RF shielding was carried out locally so that the patient was placed inside a plexiglass box covered with a copper mesh. The concept included Brainlab's VectroVision optical navigation system.

Hall *et al.* and Martin *et al.* published the University of Minnesota's iMRI-concept which was based on a 1.5 T MRI scanner (Hall *et al.* 1998, Martin *et al.* 1998). The applied scanner was a conventional diagnostic scanner with an extended scanning/operating table enabling longitudinal movement of the patient. Thus, the patient could be transferred from the imaging area to the operating area outside the 0.5 mT boundary and conventional instruments and devices could then be used. Hall *et al.* reported brain biopsies carried out in the immediate vicinity of the scanner or inside the scanner (Hall *et al.* 1999, Hall *et al.* 2000).

The Erlangen group, previously using the low-field scanner, reported their experiences in 2003 with a high-field scanner. For the surgical operation the operating table was turned through 160 degrees, and thus the patient's head was in the fringe field outside the 0.5 mT line. Transfer allowed, for example, the use of a neuronavigated microscope. Based on previous experience, the group stated that

use of the high-field system was clearly more diversified compared to using a low-field system. (Nimsky *et al.* 2003)

Recently, even higher magnetic fields have been applied intraoperatively in neurosurgery. The University of Minnesota researchers reported on applying the 3 T Philips scanner for guiding brain biopsies (Truwit & Hall 2006). Pamir *et al.* from Istanbul used a 3 T Siemens Trio MRI scanner for low grade glioma resections with the use of intraoperative proton MR spectroscopy (Pamir *et al.* 2010).

2.3.3 Clinical impact of intraoperative magnetic resonance imaging

In the early 1990s the primary reasons for development of intraoperative MRI were the assessment of brain shift, control of the resection during surgery and evaluation of intraoperative complications. (Black *et al.* 2011) Since then iMRI has mainly been used for tumor resections, but also for the guidance and control of brain biopsies (Hall *et al.* 1999) and DBS (deep brain stimulation) electrode implantations (Larson *et al.* 2011).

There are only a few systematic reviews for the evidence of the clinical impact of iMRI (Senft *et al.* 2011, Kubben *et al.* 2011 and no systematic research for longer survival time. However, regardless of used surgical method, the literature shows growing evidence of a clinical impact of gross-total macroscopic resection of gliomas on recurrent growth and patient survival (McGirt *et al.* 2009, Sanai & Berger 2008, Stummer *et al.* 2006). Theoretically low-grade gliomas could be operated achieving gross-total resections more easily because low-grade tumors are fairly well-defined, whereas high-grade gliomas grow in an infiltrative way. iMRI has been proposed to be most beneficial for surgery of low-grade gliomas (WHO I-II) where gross total tumor resection is theoretically achievable with both high and low-field iMRI scanners (Hatiboglu *et al.* 2009, Senft *et al.* 2010, Senft *et al.* 2011). Hatiboglu also showed some benefits regarding high grade gliomas, whereas Hirschberg's group stated that in grade IV tumor cases the size of the residual tumor or resection totality does not statistically increase efficacy of surgery when iMRI is utilized (Hirschberg *et al.* 2005, Hatiboglu *et al.* 2009). Kubben's group in their recently published review article showed that iMRI guided glioblastoma surgery is more effective than conventional surgical navigation guided surgery for increasing the extent of tumor resection, enhancing quality of life or prolonging survival after resection (Kubben *et al.* 2011). Nimsky stated that glioblastoma surgery with intraoperative high-field MRI guidance

showed a significant increase in median overall survival when an extent of resection of more than 98% and resections that were 78% of the intended size corresponded with a survival benefit (Nimsky 2011).

2.4 Computed tomography in neurosurgery

2.4.1 History of computed tomography in neurosurgery

The use of computed tomography has been continually developed since 1972 when engineer Godfrey Hounsfield published his results in oral presentations. In 1963 and 1964, even before Hounsfield's first CT scanner was used in 1971, physicist Allan Cormack published his mathematical theory of CT, which is still used in modern CT scanners. Hounsfield and Cormack shared the Nobel Prize in Physiology or Medicine in 1979.

The first clinical patient scanning was in October 1971 at Atkinson Morley's Hospital in South London where the first CT prototype was installed. The very first and subsequently more than 10 other intracranial tumor cases were successful when they compared scanned images and neurosurgical findings. At that time it was found that injected iodine-based contrast agent would enhance the image quality for detection of pathological findings. (Beckmann 2006)

Commercial CT scanners, based on the back-and-forth rotating gantry, were installed from 1974. The first scanners were for cranial imaging and therefore images were utilized mainly by neurosurgeons. Since then the development of CT has been continuous. Now CT scanners can be utilized for anatomical images and angiographies, the scanners can be fixed or portable, they are faster and patient comfort is good with possibilities existing for oblique slice directions and 3D reconstructions.

2.4.2 Computed tomography as an intraoperative imaging method

Computed tomography has been applied intraoperatively in neurosurgery since 1978 when the Elscint Model 719 CT scanner in Tel Aviv was utilized to control residual tumor during resection (Shalit *et al.* 1979). Engle and Lunsford published their results of nine patient cases in 1987 (Engle & Lundsford 1987). They stated that: "Although total resection of malignant brain neoplasms remained an

unrealized goal, intraoperative CT increased the surgical accessibility of malignant and benign lesions located in critical areas of the brain."

Control of the location of stereotactic instruments intraoperatively with the CT scanner was reported by Lunsford (Lunsford *et al.* 1983). They recommended combining stereotactic operating and CT scanning rooms. Intraoperative CT (iCT) was used for the first time in functional target determination by Ohye in 1984 (Ohye *et al.* 1984). The method was tentative.

During the past two decades portable head CT scanners have come into general use, but most of them are used only preoperatively for diagnostic imaging in trauma cases or in intensive care units postoperatively. (Rumboldt *et al.* 2009) However, this kind of scanner could be utilized intraoperatively as has been done in Vienna by Matula's team (Matula *et al.* 1998) and in Munich by Gumprecht and Lumenta (Gumprecht & Lumenta 2003).

Since 2009 Oulu University Hospital has utilized an orthopedic CT-like 3D-scanner, the O-arm, in neurosurgical cases as an intraoperative imaging unit for DBS electrode implantations and trigeminus neuralgia ablations and evaluated it for operations on brain tumors and intracerebral hematomas (unpublished). Recently other centers have also published their experiences with the O-arm especially in DBS cases (Caire *et al.* 2010, Shahlaie *et al.* 2011, Smith & Bacay 2011).

2.4.3 Clinical impact of intraoperative computed tomography

It has been shown that iCT can be used successfully for neurosurgical cases. Gumprecht & Lumenta from Munich published their account of four years' experience with the intraoperative mobile CT scanner (Gumprecht & Lumenta 2003). They stated that iCT is a good method for detection of residual tumor, but they believed that the neuronavigation itself is useful in most of the cases and that intraoperative imaging can be helpful only in some selected cases. Hosoda *et al.* had used iCT routinely in over 800 cases since 1997 and they found that iCT may improve the outcomes of patients with low grade gliomas (WHO II astrocytoma, oligodendroglioma, or oligoastrocytoma). They showed prolonged survival time among patients with iCT-guided operations compared to patients without iCT-guidance (Hosoda *et al.* 2011). The 5-year survival rates were 13/23 (56.5%) in the non iCT group and 20/23 (87.0%) in the iCT group ($p < 0.0001$).

2.5 Neuronavigation

Neuronavigation (or surgical navigation) is a technical tool to guide surgical procedures. In neuronavigation a spatial and transformational connection is made between the object and the image data of the object. The connection is calculated by computers. Thus, the object and its corresponding image data can be monitored with an appropriate instrument. By tracking surgical instruments the navigation system is capable of visualizing the area and propagation direction of the instrument used by the surgeon at that moment. Information is presented in real time and in three dimensions. Navigation equipment allows the surgeon to even find objects of a few millimeters in size. Stereotactic methods are not exactly neuronavigation because their use cannot be inherently monitored in real time.

Neuronavigation equipment consist of four parts:

- Patient immobilization
- Registration method
- Intraoperative localizing method
- Display device for visualizing the image data

Additionally, the systems may include:

- Software for image corrections
- Intraoperative imaging method

2.5.1 Localization methods

Mechanical localization

The first neurosurgical localizing methods were based on stereotactic frames, where localization uses the passive mechanical system and its coordinates without continuous visualization of the instrument's location and orientation. Image data is fixed to the coordinates of the stereotactic frame attached to the patient's skull, which allows the instrument to be guided into the skull along a rigid trajectory. The downside of this method is the limitation of aiming the instrument at a single target or multiple targets along the same trajectory. This limits the number of clinical applications. (Redfern 1993, Watanabe 1993, McInerney & Roberts 2000)

Digital measurement techniques using mechanical positioning methods are based on the length of the articulated arms, the positions of the joints and the pointing device at the end of the arm. Positions of the joints were determined by potentiometric (Watanabe 1993) or optical (Oikarinen *et al.* 1993) position sensors. The neuronavigator developed at Oulu University Hospital was a pioneer of modern technology, because for the first time during surgery it allowed simultaneous co-planar presentation of pre-operative MR and intraoperative ultrasound images (Koivukangas *et al.* 1993).

Actively controlled devices, such as robots, can be included in the group of mechanical navigators. Robotics has been utilized for example in surgical microscopes, surgical manipulators and positioning in radiosurgery. (Kuo *et al.* 2003, Louw *et al.* 2004)

Electromagnetic localization

An electromagnetic localizing method is based on the relationship of the magnetic field strengths between the transmitter near the patient's head and those measured by the sensor attached to the applied instrument. Magnetic field strength decreases as a function of distance R ($1/R^3$).

The position of the instrument's tip, such as a flexible endoscope, can be determined by one sensor at the tip of the instrument (Zaaroor *et al.* 2001). In addition, the direction of the instrument can be determined if two or more sensors are attached to a rigid instrument (Kato *et al.* 1991, Manwaring *et al.* 1994, Suess *et al.* 2001).

The magnetic tracking method has the advantage that it does not require a direct line of sight between the transmitter and the receiving sensors, because magnetic fields penetrate a biological medium. One problem is the inductive interaction of the electromagnetic fields in conductive materials, such as steel and aluminum, near the operating area. Alternating magnetic fields induce eddy currents in conductive materials that interfere with the transmitter field (Nixon *et al.* 1998, Suess *et al.* 2001). The problem is significant when using continuous alternating current in the transmitting mode (Kato *et al.* 1991). A continuous electromagnetic field creates a continuous disturbance field. Induced disturbance fields attenuate rapidly when transmitting fields are generated using pulsed direct current. (Manwaring 1993).

Acoustic localization

Acoustic localization is based on sound source localization using the triangulation principle. Transmitters attached linearly or in a two-dimensional plane to the instrument send repeating ultrasonic pulses which are detected by three or more microphones (Roberts *et al.* 1986). The time delay between pulse generation and detection is measured and the position of the instrument and its tip is determined using the triangulation principle.

Ultrasound-based localization is prone to errors. There must be a direct connection between the transmitter and the receiver. Dead spots are a potential source of reflections that increase tracking error. Errors are also caused by noise in the environment, and accuracy is influenced by changes in temperature, humidity and the medium where the ultrasound is propagated (Barnett *et al.* 1993a, Barnett *et al.* 1993b, Barnett *et al.* 1993c).

Optical localization

Optical localization is based on optical, infrared (ir) cameras monitoring passive light-reflecting spheres or active optical transmitters fixed to the used instrument or tool. In active navigation infrared emitting diodes are used (Gamache 1997, Germano *et al.* 1999). In the passive method, the light source is in the camera following the reflected infrared light from the reflecting spheres (Vahala *et al.* 2001). Direction, position and rotation of the used instrument can be determined by the plane formed by three or more marker points (Lango 2000). The time lag between light transmission and reception is the basis for the instrument's location and orientation. For different instruments unique configurations of the reflecting spheres can be used to tell what instrument is in the operating area. This method can be used to monitor multiple instruments simultaneously.

In the active method, the diodes require a power source, which complicates the method particularly by the use of cables or batteries. In the passive method, the instrument and its sensor operate without electricity, so the instruments and the trackers can be sterilized. This method requires direct line of sight between the infrared camera and the instrument trackers.

2.5.2 Registration methods

Registration means that the three-dimensional image data obtained from different imaging modalities and the physical object are linked to each other. Three methods can be used to combine images and the object: point-to-point, surface matching, and direct coordination transfer methods.

Point-to-point method

The point-to-point method is the most commonly used registration method. It is based on the idea of finding corresponding coordinates between images and the patient by pointing at the corresponding points on the patient and in the image data with the navigation instrument. Coordinates are used to calculate the geometric changes between volumes of the image data and of the patient. Selected points can be either internal or external. Internal points are accessible anatomical structures that appear on the images clearly. External points are artificial markers attached to the skin or to the bone. (Maurer & Fitzpatrick 1993, Evans *et al.* 1993, Maurer *et al.* 1997, Lewis *et al.* 1998, Edwards *et al.* 2001)

Surface matching method

The surface matching method is based on the coordinates of corresponding contours in a segmented 3D image data, and in the contours of the patient's head. Coordinates are used to calculate the relations between an object and the segmented image volume. (Evans *et al.* 1993, Maurer & Fitzpatrick 1993) A contour map of the patient's head can be determined by touching the head with a pointer or a laser instrument (Henderson *et al.* 1994, Schlaier *et al.* 2002, Raabe *et al.* 2002).

Direct coordination transfer method

In the direct coordination transfer method the registration between the image data and the physical object is based on the coordination of the scanning system. If the navigator can see the positions of the scanner and the patient's head using trackers attached to the scanner and to the head holder, respectively, during scanning, the coordinates of the head and the obtained images can be registered automatically.

The method can be used only with intraoperative imaging systems. (Vahala *et al.* 2001, Vahala 2002)

2.5.3 Immobilization methods

Regardless of the localization and registration methods used the existing linkage between image data and the patient's head must remain. Linkage is maintained by fixing the patient's head so that its movement is prevented, or in a way that head movement can be followed.

Stereotactic frames

A stereotactic frame is used in operations where accurate positioning of small objects is required. The frame is attached to the head with invasive skull pins. The coordinates of the surgical object relative to the origin of the frame are calculated on the basis of coordinate calibration markers seen in the MR or CT images. The closed structure of the frames limits applications mainly to brain biopsies and implantations of deep brain stimulation electrodes.

Head holders

The most commonly used immobilization method in brain tumor resections is to fix the head to the head holder by three or four skull pins. The open design of the head holders allows the surgeon access to the region of surgical interest. The patient tracker can be attached to the head holder, thus the place of the head holder, i.e. the place of the head, can be navigated by following the patient tracker, and therefore head position can be changed after the registration phase.

2.5.4 Sources of errors

In neuronavigation it is essential to produce the correspondence between the physical object and the image data as accurately as possible. Various factors that cause inaccuracies need to be taken into account. These factors can be divided into four categories according to origin: technical accuracy of the used imaging modality, technical localization accuracy of the navigation system, technical accuracy of the registration method and intraoperative changes in a patient (Kaus *et al.* 1997, Steinmeier *et al.* 2000, Edwards *et al.* 2001).

Each factor affects the others. Generally, only the sum of the inaccuracies caused by the technical accuracy of the imaging modality, technical localization accuracy of the navigation system and technical accuracy of the registration method can be determined (Schiffbauer 1999, Marmulla *et al.* 1998). Intraoperative changes occur gradually as the operation progresses, and they may be compensated by updating the navigation system image data with intraoperative imaging modalities. Recently Shamir *et al.* published their results of total inaccuracies when implanting ventricular catheders using a commercial neuronavigation system (Shamir *et al.* 2011). According to their results, the mean localization errors at the target and entry point locations were 5.9 ± 4.3 mm and 3.3 ± 1.9 mm, respectively.

Technical accuracy of imaging modality

The most commonly applied imaging modality in neuronavigation, MRI, is particularly sensitive to spatial inaccuracies. Spatial inaccuracy of image data due to the gradient's nonlinearities and to static magnetic field strength and its inhomogenities may be greater than voxel size (Yu *et al.* 2001). Also, the structure of the scanned object, eddy currents inside the object and local effects caused, for example, by the susceptibility differences at the air-tissue interface can influence spatial accuracy. (Parizel 1994, Schenck 1996, Brommeland & Hennig 2000, Koivula 2002)

Localization accuracy of the neuronavigator

Localization inaccuracies depend on the technology used. In the optical method, mechanical vibrations and the distance between the camera and the instruments can cause inaccuracy (Kaus *et al.* 1997). Kaus *et al.* stated that the maximum localization error detected was 0.55 ± 0.29 mm, with the z direction (distance to the camera array) being the most erroneous coordinate. Our own results showed slightly smaller errors (Koivukangas *et al.* 2011) than Kaus *et al.*'s, but we also found also that the z-direction is the most error prone. Also Wiles *et al.* reported comparable localization inaccuracies of the optical tracking system (Wiles *et al.* 2004).

Technical inaccuracy of magnetic localization has been shown to be a little higher, but at the same submillimeter level as the inaccuracy of the optical

localization method (Mascott 2005). Mascott showed that the difference in the errors was within 0.5 mm.

Accuracy of registration method

How accurately the equivalence between the image data and the physical object is maintained is the primary factor in registration accuracy. The accuracies of the image data and localization methods and shape and size of the corresponding points influence the total registration accuracy. (Edwards *et al.* 2001)

According to results of Woerdeman *et al.* mean registration accuracy using fiducial markers, surface matching and anatomical landmarks were 2.49 ± 1.07 mm, 5.03 ± 2.30 mm and 4.97 ± 2.29 mm, respectively (Woerdeman *et al.* 2008). Furthermore, Shamir *et al.* published registration errors based on fiducial markers and surface matching of 3.9 ± 1.2 mm and 4.1 ± 1.6 mm, respectively (Shamir *et al.* 2009).

Intraoperative changes

The benefits of neuronavigation utilizing preoperative image data deteriorate as a result of changes occurring during surgery. The most significant and well-known source of such inaccuracies is tissue changes due to resection and fluid leakage, called "brain shift" (Roberts *et al.* 1998, Maurer *et al.* 1998, Dorward *et al.* 1999). Changes after image data collection and before registration could also cause errors.

Based on a series of 28 patients Roberts' team (Roberts *et al.* 1998) presented their conclusions regarding factors causing brain tissue shift. They argued that cortical shifts that occurred were in the order of about 10 mm relative to the control point, and, despite the position of the head, changes are most significant straight downward along the gravitational force. Maurer *et al.* (1998) suggested that brain tissue shifts are minimal in the midline, the tentorium, contralateral hemispheres and ipsilateral space when they are further than 10 mm from the operating area. Maurer also proposed a number of factors that affect brain tissue changes, such as the anesthetics and steroids used, the osmotically active agents, tumor size, tumor location, craniotomy size, extent of resection and brain atrophy. Nabavi *et al.* have reported brain shift of up to 50 mm (Nabavi *et al.* 2001).

The effects of brain shift have been compensated for in a variety of ways, such as the use of calculation algorithms (Ferrant *et al.* 2002), intraoperative

magnetic resonance imaging (Nimsky *et al.* 2000, Nabavi *et al.* 2001) and the registration of preoperative MR images to intraoperative ultrasound images (Roche *et al.* 2001, Pennec *et al.* 2001, Rasmussen *et al.* 2007).

3 Aims of the study

The purpose of the present study was:

1. To investigate the technical and clinical feasibility of low-field magnetic resonance imaging guidance in brain tumor surgery
2. To explore the inversion recovery magnetic resonance imaging sequence to attenuate the magnetic resonance signal of edema for better differentiation of gross tumor volume
3. To study the accuracy and feasibility of the multimodal combination of intraoperative magnetic resonance imaging and intraoperative ultrasound imaging
4. To evaluate a new intraoperative computed tomography imaging system as a targeting and controlling method in stereotactic neurosurgery

4 Patients, materials and methods

4.1 Patients

This study was carried out at the Department of Neurosurgery at Oulu University Hospital. All patients were selected according to medical need. Studies I-III were part of the "Intraoperatiivinen MRI" research which was going on at Oulu University Hospital and were approved by the local ethics committee. The O-arm assisted procedures itself required no new experimental actions. Since the validation was done the O-arm scanning replaced the conventional CT imaging that had been routinely used. A summary of the patients is presented in Table 1.

Table 1. This study included 68 different patients. Most of the cases were tumor resections.

Study	N (m / f)	Age / years	Diagnosis	Operation
I	34 (22/12)	26–88	13 low-grade gliomas, 18 high-grade gliomas, 3 others[a]	27 resections, 5 biopsies, 1 hematoma evacuation, 1 AVM removal
II	28 (18/10)	9–76	9 low-grade gliomas, 14 high-grade gliomas, 5 others[b]	28 brain tumor resections, 25 different patients (three patients were operated and scanned twice)
III	1 (0/1)	57	1 high-grade tumor	resection
IV	8 (5/3)	34–72	Advanced Parkinson's disease, dystonia, MS tremor, Parkinsonian tremor, acute intracranial hematomas	6 DBS implantations, 2 patients to evaluate visualization of acute intracranial hematomas

N, number of cases; m, male; f, female; AVM, anteriovenous malformation; MS, multiple sclerosis; DBS, deep brain stimulation

[a] chronic subdural hematoma, plasmacytoma, anteriovenous malformation;

[b] two non-diagnostic tissues, metastatic tumor, plexus papilloma, dysembryoplastic neuroepithelial tissue

4.2 Materials

In this doctoral thesis practical intraoperative imaging concepts were developed for brain tumor resections and stereotactic procedures. The feasibility and accuracy of the concepts were evaluated. Used materials and methods are summarized in Table 2, and more specifically described in the text.

Table 2. Four different intraoperative imaging concepts were applied to delineate and localize region of surgical interest.

Study	Purposes	Intraoperative imaging methods	Concept included
I	To investigate feasibility of the low-field MRI scanner in brain tumor surgery	Low-field MRI, (US)	Low-field iMRI-OR, Arm-based LIS-navigator, IOUS
II	To explore the inversion recovery sequence to obtain better delineation of gross brain tumor volume	Low-field MRI	Edema suppression inversion recovery in low field iMRI environment
III	To study feasibility and accuracy of two combined intraoperative imaging modalities	US, low-field MRI	Optically navigated IOUS in iMRI environment, Optical iPath-200-navigator, US-MRI-phantom
IV	To evaluate and form a new intraoperative imaging modality for targeting and controlling stereotactic operations	CT	iCT, Leksell stereotactic system, Spatial and technical accuracy phantoms

MRI, magnetic resonance imaging; US, ultrasound imaging; iMRI, intraoperative magnetic resonance imaging; OR, operating room; LIS, Leksell Index System, arm-based navigation system; IOUS, intraoperative ultrasound imaging; iCT, intraoperative computed tomography;

4.2.1 The low-field iMRI scanner

The iMRI scanner used in studies I-III was a horizontally open resistive Philips Outlook Proview low-field 0.23 T scanner (Philips Medical Systems MR Technologies Finland, Inc.). The scanner could be turned off and then on again with a relatively short 6-minute ramp-up time. The scanner's imaging volume accuracy was ±5 ppm or better inside a sphere of 40 cm diameter centered on the scanner's isocenter, which was equivalent to 1.02 mm with the used 3D MRI sequence.

Fig. 1. The Proview scanner was a C-shaped iron core electromagnet with a 44 cm patient gap. The advantages of the scanner included the possibility to turn it off, with a 6-minute ramp to imaging time, and a fully detachable patient couch that was movable on rails. Neurosurgical tumor resection was performed outside the MR scanner. Use of non-MRI-compatible instruments and devices (such as the ultrasound scanner, left) during a neurosurgical operation was rendered possible by the resistive magnet's turn-off feature. One fiber optic and two single surgical lights, four anesthesia gas inlets, 48 sockets and filtered air ventilation complete the operating room environment.

4.2.2 The IOUS scanner

The US scanner was an Aloka SSD-1700 (Aloka Co., Ltd, Tokio, Japan) with a 7.5 MHz neurosurgical probe (UST-987-7.5). The imaging properties such as amplification, contrast, frequency and scanning depth were adjusted subjectively for optimal image quality.

4.2.3 The iCT system, the O-arm

The Intraoperative computed tomography system, the O-arm (Medtronic Inc., Louisville, CO, USA) (Fig 2), was a surgical, mobile 2D/3D x-ray imaging system optimized for spinal and orthopedic surgery. Scanning was based on a flat panel detector and cone-beam technology producing 196 slices in 13 seconds in the standard mode, 382 slices in 26 seconds in the high definition mode, and 196 slices in 26 seconds in the enhanced mode, the latter specially designed for cranial solutions. Pixel size was 0.415 × 0.415 mm with a slice thickness of 0.833 mm. The size of the scanned cylindrical 3D volume was 21 cm × 16 cm (diameter × length), which was less than required for obtaining a full scan of the Leksell CT coordinate indicator box.

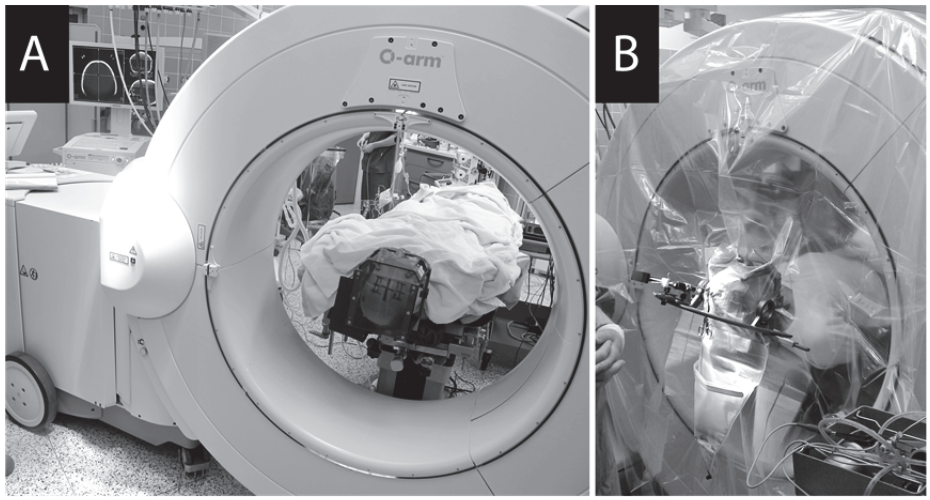

Fig. 2. The O-arm was a movable CT-like scanner (A). With automated positioning it could be easily placed around the patient to obtain 3D scanning or 2D fluoroscopic images in desired directions, and repeatedly when necessary (A,B).

4.2.4 Navigation systems used in studies

Arm-based LIS-navigator

In study I, the mechanical arm-based LIS (Leksell Index System, Elekta Ab Stockholm, Sweden) neuronavigator was used in three cases until the optical

iPath was ready for clinical applications. The LIS neuronavigator was specially made by Elekta Ab for the Oulu Clinic for Neurosurgery and several other centers in 1994. It had been invented as one of the early neuronavigators in the Neurosurgical Research Unit (Koivukangas *et al.* 1993a, Koivukangas *et al.* 1993b, Oikarinen *et al.* 1993) and commercialized as a joint project by Elekta Ab and Onesys Oy, Oulu, Finland (Eureka Project 714, EU: 1992). The LIS guided the surgical approach and initial resection based on the preoperative images, and it could be updated by co-planar intraoperative US and MRI data. The registration between an image dataset and real patient anatomy was based on the manual point-to-point registration method (Schiffbauer 1999).

Optical iPath-200

The iPath-200 package (Philips Medical System MR Technologies Finland Inc., Vantaa, Finland) was developed on the basis of the tool coordinated system (TCS) of the LIS neuronavigator as a joint project by the Neurosurgical Research Unit, Oulu University Hospital, and Philips. The package consisted of an optical tracking system and a 36-inch video projector screen (resolution: 1280 x 1024) with a separate in-room control panel. The optical tracking system was based on CCD (charge coupled device) infrared cameras, which followed the reflecting spheres fixed to the head holder, the scanner and the instruments. The commercial iPath was fitted with a patient tracker and supplementing software, which enabled navigation outside the scanner and visualization using the TCS, showing 3D multiplanar reconstructions related to the axis of the used instrument.

The navigation system registered the 3D dataset and patient's anatomy automatically. This was based on correspondingly oriented coordinates of the image data and the scanner image volume, the common origin being at the isocenter point of the scanner. This registration method did not require surface matching or point-to-point registration markers. The patient could be moved from the scanner after the transformation from the magnet coordinates to patient coordinates had been done (Vahala *et al.* 2001, Vahala 2002).

Stereotaxy

In study IV, the G-model Leksell Stereotactic System (LSS) with the Leksell CT coordination indicator box (Elekta Ab, Stockholm, Sweden) was used as the guiding method. The LSS could be used with aluminum (insulated or non-

insulated) or carbon fiber posts and reusable aluminum or titanium fixation screws. As the physical dimensions of the CT coordination indicator box were larger than those of the scanning volume of the O-arm, some small extra markers of copper were added to the indicator box to help the merging of the limited O-arm dataset of the patient to the full generic CT dataset of the indicator box imaged without the patient.

FrameLink stereotactic calculation software (Medtronic Inc., Louisville, CO, USA) was used for planning the trajectories on MR images usually a day before the operations and for calculating the coordinates of the target at the beginning of the operation. FrameLink was also used for intraoperative control at the end of the operation when the postoperative O-arm 3D-dataset was merged with the surgical plan. StealthViz medical image processing software (Medtronic Inc., Louisville, CO, USA) was utilized after the patient was scanned with the coordinate indicator box in the O-arm. With StealthViz software the incomplete scanned dataset of the patient with the coordinate indicator box and the full volume dataset of the CT coordinate indicator box without the patient generically scanned with diagnostic CT in the radiological department could be merged and combined into one single DICOM (Digital Imaging and Communication in Medicine standard, National Electrical Manufacturers Association NEMA, Rosslyn, VA, USA) dataset. Both software programs were installed in the StealthStation S7 navigator (Medtronic Inc. Louisville, CO, USA) and used in the operating room.

4.2.5 Phantoms

All phantoms were custom designed and manufactured for this doctoral thesis. The US-MRI-phantom was used in study III and phantoms for spatial and technical accuracy measurements were used in study IV.

The US-/MRI-phantom

The US-/MRI-phantom was an object whose structure was known exactly and could be visualized with both US and MRI. The phantom included three parts: a waterproof acrylic cube (170 × 170 mm), a 7 × 7 acrylic rod matrix (diameter of rods 4.0 mm, separations 20.0 mm from center point to center point in vertical and horizontal directions) and an adapter for US probe fixation. Acrylic plastic (PMMA; polymethylmethacrylate) was chosen because of a magnetic susceptibility value near to that of water to minimize distortions in the MR

images. Moreover, metallic particles caused in machining (drilling, sawing, etc.) were carefully washed away at the end of production.

Phantoms for spatial and technical accuracy measurements

In study IV, two different phantoms were designed and applied for accuracy assessment; one for demonstration of the spatial accuracy in the scanning volume and one for determination of the concept's technical accuracy. In both phantoms, parts which were to be scanned within the O-arm were made of acrylic plastic (PMMA, polymethylmethacrylate). PMMA has long been used in medical phantoms because of its properties, e.g. it is stable for changes in the ambient environment, it is artefact-free and it can be scanned with different imaging modalities.

The spatial accuracy phantom included equally distributed acrylic plastic rods in three different levels in known positions (Koivukangas *et al.* 2011) The rods were visualized with the O-arm images and could be used for determination of spatial accuracy in the 3D-volume when the positions of the rods are compared to their real positions.

The technical accuracy phantom, made of acrylic plastic, was designed to be fixed to the Leksell frame and to simulate a real patient with the artificial points of AC (anterior commissure), PC (posterior commissure) and STN as targets.

4.3 Methods

4.3.1 Low-field intraoperative MRI

The low-field iMRI unit was planned and applied in 34 neurosurgical cases. The unit had to be equipped as a full scale operating room (Fig 1) and it had to also enable several MR imaging sessions during a neurosurgical operation as well as multimodality patient monitoring and imaging, including ultrasound imaging. The C-shaped resistive electromagnet was chosen to allow the magnetic field to be turned off during the operation. This made it possible to use non-MRI-compatible devices and instruments in the combined imaging and operating room during surgery.

4.3.2 MR scanning for edema attenuation

Study II was divided into two parts. First, the theoretical value for the time of inversion (TI) that attenuates radio frequency signal from edema was tested in three different patients by using inversion recovery (IR) sequences with four different TIs. RF-signal intensities of edema, brain tissue and tumor were measured with analyzing tools included in the MR-scanner control software. The signals from the edematous regions were subtracted from background noise and presented as a function of TI. Least square fits were calculated through the data points using a logarithmic equation.

Second, the best edema suppression of the IR sequences of various TIs was assessed from the neurosurgical point of view in brain tumor operations by the neurosurgeon and neuroradiologist.

Application of theory

For inversion recovery sequences where time of repetition (TR) is much longer than longitudinal relaxation time T_1 ($TR >> T_1$) the inversion time for nulling of a signal in the IR sequence is

$$TI = T_1 \times \ln 2 = 0.69 \times T_1. \quad (1)$$

According to Bottomley *et al.* the T_1 relaxation times can be derived from the formula

$$T_1 = A\nu^B,$$

where A and B are the tissue specific constants, and ν is the resonance frequency for protons. At 0.23 T field strength, ν = 9.8 MHz and for brain edema A = 0.00785 and B = 0.2745 with a standard deviation of 23% (n = 32) (Bottomley *et al.* 1987).

This led to T_1 = 651 ms for brain edema in a 0.23 T magnetic field. Incorporating this value into the first equation gave a TI of 451 ms for edema suppression. When the range of standard deviation for A and B was taken into account, the range of TI that suppresses edema could be expected to be 348 ms to 555 ms.

Imaging protocol

An inversion recovery sequence with different inversion times was added to the MR imaging protocol for 25 neurosurgical patients. Three patients underwent two separate operations each and thus were scanned twice. The IR sequences consisted of a selective 180º inversion pulse followed by a fast spin echo (FSE) sequence. The axial image plane with 5 mm slice thickness and 1 mm gap between slices was applied for all IR sequences. Image reconstruction utilized magnitude encoding, where the intensity of the signal was shown as an absolute value.

Imaging was performed on the day before and two days after the operation. Eight patients were also scanned during an intraoperative imaging session with an IR sequence (TI 600 ms or 800 ms). Pre- and postoperative imaging was performed with an array receiver coil and intraoperative imaging with an integrated head holder receiver coil.

4.3.3 Multimodal combination of iMRI and IOUS scanning

The ultrasound imaging was interlinked to the navigation system with the instrument tracker (IT) fixed to the US probe and a specific transformation matrix file included in the navigation software. The materials in the IT were carefully chosen and medically accepted: plastic (Ultem®, General Electric Plastics, Pittsfield, MA, United States), titanium, aluminum and brass. For calibration the pointer included also polyacetal plastic (POM, polyoxymethylene). Magnetic susceptibility and electric conductivity values of materials were taken into account to achieve MR-compatibility. Construction of the IT aimed to be ergonomic: the IT could not disturb use of the US probe, the reflecting spheres should be visible to the ir-camera in a wide angle, and fixation to the US probe had to be tight and simple. The file added to the navigation software specified a transformation matrix between the axial surface point of the US scanning axis and the configuration of the reflecting spheres. Hence the navigation system recognized the IT and its orientation and location relative to the image data.

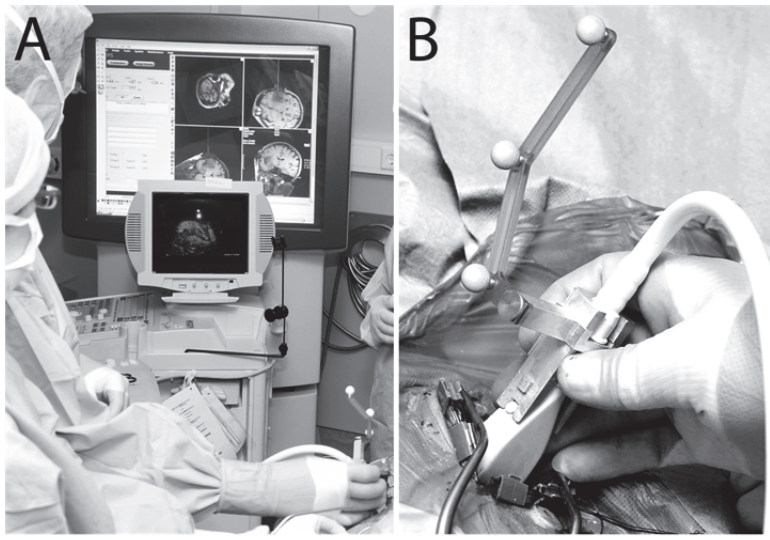

Fig. 3. The sterilizable ultrasound imaging probe and the optical passive IT were fixed together ergonomically (B). The surgeons could see both modalities at the same time on separate monitors (A). The MRI reconstruction in the left lower corner of the in-room monitor was equivalent to the ultrasound image. The ir-camera was situated to the left of the ultrasound scanner and it could follow the ultrasound tracker constantly in a wide range of angles.

The intraoperative MRI scanning was carried out as follows: the patient tracker was fixed to the scanned object (patient or US-/MRI-phantom), the object was positioned as near the isocenter as possible and magnetic field homogeneity was adjusted. For navigation a 3D MRI data set was collected with a T_1-weighted 3D field echo sequence FE-3D (TR/TE 27/10 ms; flip angle, 45; field of view, 250 × 250 mm; matrix, 250 × 250 pix; averages, 1; and slice thickness/separation, 3.0 mm/3.0 mm). For the study of corresponding measurements, slice orientation was exactly aligned with the ultrasound plane. In operations the slice orientation was selected parallel with the planned surgical approach.

4.3.4 iCT-guided stereotactic operations

In the OR, right after the Leksell stereotactic frame (G-model, Elekta Ab, Stockholm, Sweden) was fixed to the patient's head and the patient was positioned in a comfortable position on the operating table, the O-arm was used to

collect a 3D dataset in the enhanced mode for calculation of the target coordinates. After scanning the O-arm was moved to its parked position.

The 3D dataset was imported into the StealthViz software of the S7 navigation system (Medtronic Inc. Louisville, CO, USA). With the StealthViz software the patient specific O-arm dataset and the generic CT dataset from the coordinate calculation box without the patient were merged to become one single dataset (Fig 4). The new dataset was exported into the FrameLink stereotactic calculation software (Medtronic Inc. Louisville, CO, USA), which was able to recognize all nine rods on the plates and to formulate coordinates inside the brain. In FrameLink, preoperative MRI datasets were then merged to the O-arm dataset. Coordinates of the selected targets were calculated based on the rods in the O-arm images.

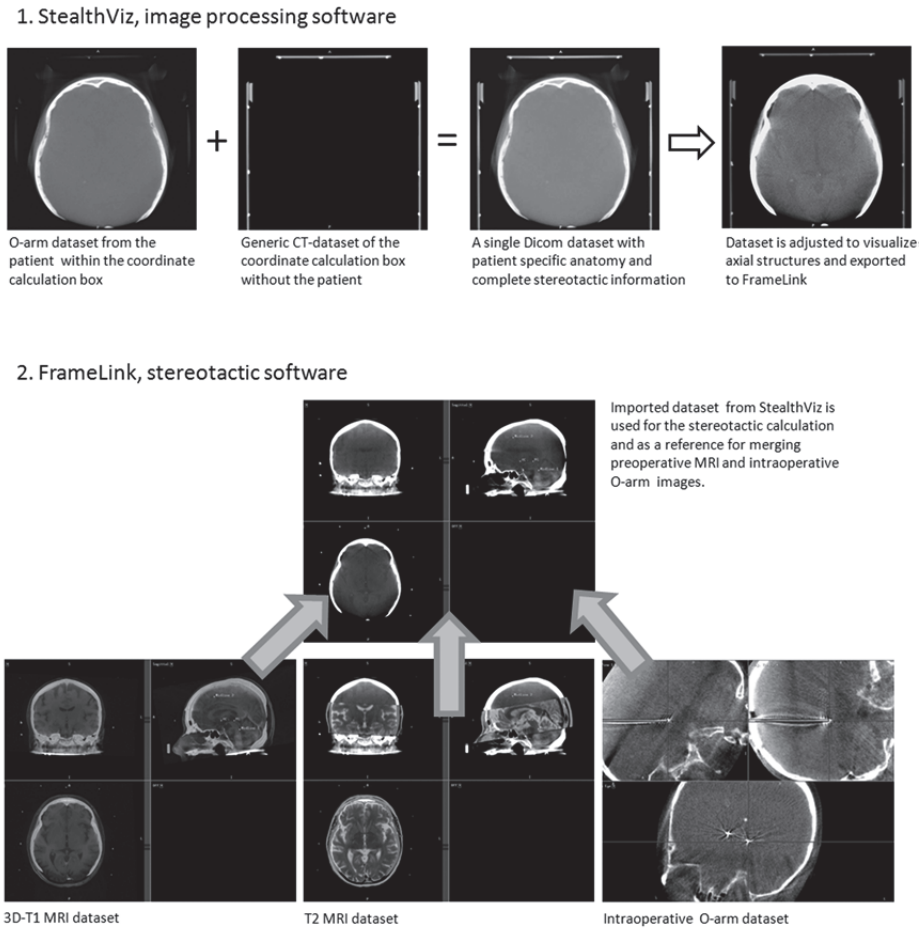

Fig. 4. StealthViz and FrameLink softwares were both needed during operation to enable calculation of the target coordinates and verification of the final position of the implanted instruments.

The surgical operation was done as usual with O-arm control as needed. The automated positioning system helped to park the gantry of the O-arm away from the surgical area and then to drive it back over the patient's head when 2D or 3D images were needed, so the control images could be taken in seconds. The flat panel detector offered good quality wide area 2D images for control of localization of DBS, MER (microelectrode recording) or thalamotomy electrodes. Image quality was good for intraoperative requirements and ensured exact location of the electrodes.

At the end of the operation a 3D dataset was scanned. It showed the exact locations of implanted electrodes. The dataset could be merged with the preoperative plan to compare the planned and the real locations of the DBS-electrodes.

Generic dataset of the coordinate indicator box

The diagnostic CT scanner (Siemens Somatom Sensation 64 with Syngo CT2007S, Siemens AG, Erlangen Germany) was used once to scan a full dataset for the CT coordination indicator box without a patient. The scanning parameters were 120 kVp, 380 mAs, 512 × 512 × 0.6 mm within the reconstruction diameter of 271 mm. One dataset was generic for all phantom tests and patient cases.

Preoperative MRI datasets

The O-arm was a spinal and orthopedic imaging system optimized for bony structures. Its soft tissue contrast without further development was insufficient to reliably determine deep brain structures. Therefore patients were scanned preoperatively with magnetic resonance imaging (GE, Signa HDxt Twinspeed 1.5 T, Waukesha, WI, USA) for the preoperative planning and to ensure accurate localization of the anterior and posterior commissures on axial 3D fast SPGR (spoiled gradient recalled) T_1-weighted images with the contrast agent (repetition time, 7 ms; echo time, 2 ms; flip angle, 10 degrees; averages, 1; field of view, 300 × 300 mm; matrix, 256 × 256 pixels; slice thickness, 1.5 mm; separation, 1.5 mm) and to verify STN anatomically on the axial fast spin echo T_2-weighted images with the contrast agent (repetition time, 2800 ms; echo time, 87.6 ms; flip angle, 90 degrees; averages, 3; field of view, 300 × 300 mm; matrix, 256 × 256 pixels; slice thickness, 2.0 mm; separation, 2.0 mm).

Accuracy assessment

The spatial accuracy phantom was scanned with the O-arm and the positions of the rods were compared to their real positions. The technical and methodological accuracy of the concept was calculated by running through the whole protocol using the technical accuracy phantom. This included imaging, planning, and calculations of coordinates and placement of the instruments. Quantitative accuracy could be calculated quantitatively in the X, Y and Z directions since the

exact coordinates were known, and qualitative accuracy could be visualized with the phantom.

5 Results

Four different feasibility studies of intraoperative imaging methods for delineation and localization of the region of surgical interest showed advantages and disadvantages of the used methods. Results are summarized in Table 3 and 4 and detailed in the text.

Table 3. Advantages and disadvantages of four different methods used for image guided surgery.

Subject	Low-field iMRI-OR	Low-field EDAIR	Optically navigated IOUS and iMRI	iCT guided stereotaxy
Price	~1 000 000 eur	No extra costs	Extra ~200 000 eur	~800 000 eur
Most important advantages	Possibility to update MRI data set for navigation to guide and control the operation	Important additional data to conventional low-field MRI sequences, especially in cases of non-contrast-enhanced tumors	IOUS can visualize surgical area in real-time and it can be combined to preoperative or intraoperative MR images	DBS operation can be targeted and controlled accurately during operation
Most significant disadvantages	Magnetic fringe fields, MRI scanner sensitive to electromagnetic interference	Signal intensity is low with a surgical head coil	Separate monitors	Low soft tissue contrast, radiation doses
Requires specialized operator	Yes, radiographer and radiologist	Yes, radiographer and radiologist	No	Yes
Ionizing radiation	No	No	No	Yes
Imaging method can be used for radiological interventions	Yes	No	Yes	Yes
Imaging method can be applied in other surgical specialities	Rarely	No	Rarely	Yes

iMRI, intraoperative magnetic resonance imaging; OR, operating room; EDAIR, edema attenuation inversion recovery; IOUS, intraoperative ultrasound imaging; iCT, intraoperative computed tomography; DBS, deep brain stimulation; T_1-w, longitudinal relaxation time weighted

Table 4. Physical parameters of four different methods used for image guided surgery.

Subject	Low-field iMRI-OR	Low-field EDAIR	Optically navigated IOUS and iMRI	iCT guided stereotaxy
Scanning volume	Sphere of 26 cm diameter, when using the intraoperative head coil	260 × 260 mm^2	One US slice (scan angle of 65º, max. curvature radius of 20 cm) oriented in the same plane with a corresponding MRI slice	Cylinder with a length of 15 cm and a diameter of 21 cm
Image Resolution	1.0 × 1.0 mm^2	1.02 × 1.02 mm^2	n/a	0.415 × 0.415 mm^2
Slice thickness	3.0–5.0 mm	5.0 mm	n/a	0.833 mm
2D/3D	2D/3D	2D	2D-US combined to 3D-MRI	2D/3D
Soft tissue contrast	Good	Good, additional information to conventional low-field MRI data	Better than MRI alone	Low
Scanning time	At least 6 min (3D T_1-w)	~3 min	Real-time	26 sec (3D)

iMRI, intraoperative magnetic resonance imaging; OR, operating room; EDAIR, edema attenuation inversion recovery; IOUS, intraoperative ultrasound imaging; iCT, intraoperative computed tomography; T_1-w, longitudinal relaxation time weighted

5.1 Intraoperative MRI in neurosurgery

5.1.1 MR imaging

Study I included the very first iMRI cases during February 1999 – September 2000. During that 20-month period intraoperative MRI was applied consecutively in 34 neurosurgical operations having 51 intraoperative MRI sessions. Intraoperative MR imaging was needed in 18 cases for either orientation to tumor (2) or open biopsy site (1), or determination of residual tumor (15). For 11 (61%) of these cases, intraoperative imaging changed the progress of the operation. Another significant indication for imaging was exclusion of early postoperative

complications (19 cases). MR imaging sequences run for intraoperative imaging are listed in Table 5.

Table 5. Intraoperative magnetic resonance imaging sequences for tumor resection control.

Weighting	Type	TR (ms)	TE (ms)	TI (ms)	FOV (mm)	Slice thickness (mm)	Number of slices	Scan time (min:sec)
T1	FSE	480	20	-	250	5.0	16	4:36
T1	FE3D	27	10	-	250	3.0–5.0	24–43	2:55–6:13
T2	FSE	4300	126	-	250	5.0	24	4:35
T2	IRFSE	6250	100	2200	250	5.0	20	6:40

FSE, fast spin echo; FE3D, three-dimensional field-echo; IRFSE, inversion recovery fast spin echo; TR, repetition time; TE, echo time; TI, inversion time; FOV, field of view

The image quality – analyzed by neurosurgeons – was adequate for the intended use. Despite the low magnetic field strength, which is less sensitive to magnetic field disturbances, some MRI-compatible neurosurgical instruments made of titanium alloy caused image distortions and had to be removed before imaging.

The shut-down feature of the scanner was routinely used, and the first intraoperative images were usually scanned immediately after the 6-minute ramp-up time. However, the magnetic field was stable for adequate image quality.

5.1.2 Procedures

Within 20 months (February 1999 – September 2000), 27 brain tumor resections, 5 brain tumor biopsies, 1 extirpation of an arteriovenous malformation, and 1 hematoma evacuation were carried out in the intraoperative MRI suite. There were no complications due to the use of the advanced intraoperative imaging technology.

Twenty-eight of cases were operations for glioma, most of them (23) being resections. To yield valuable information for optimized tumor resection, five resections were performed as awake craniotomies with cortical stimulation of the speech or sensorimotor, or of both, areas. For two of the resections, electrocorticography and depth electrode registration were used to localize epileptic foci and to control the effects of tumor resection.

IOUS was applied to provide multimodal information during 20 of the 27 tumor resections and in two brain biopsies. IOUS was helpful in planning and modifying the surgical approaches. Although it cannot compete in brain tissue

contrast with MR images, it provided better real-time visualization of pulsating arteries, cystic tumor components and calcifications. In staged operations, IOUS also gave real-time information between the MR imaging sessions. Furthermore, the use of other essential non-MRI-compatible instruments and devices (e.g. microscope, arm-based navigation, drill, suction and diathermy) was possible when the magnet was turned off. As detailed above, intraoperative MRI served to rule out neurosurgical intra- and postoperative complications and to control the extent of tumor resection.

LIS was used in three cases. In two operations, we tested the new version of the optical navigation system, which was capable of tracking the instrument position outside the MR imaging space. During brain biopsies, intraoperative MRI combined with the optical tracking system offered real time information on the location and trajectory of the biopsy needle.

5.2 Edema attenuating inversion recovery (EDAIR) MRI sequence to determine gross tumor volume

Results in this section were published in study II describing results in three patient cases.

RF-signal from the edematous region could be attenuated with an inversion recovery MR-sequence, as the relaxation time of the edematous region is different compared to tumor tissue or healthy brain. Overall, IR sequences with TI between 406–721 milliseconds were found promising for edema suppression at 0.23 T. However, the range of sufficient TI value varied from case to case (see patient cases 1, 2, and 3 and Fig 8, 10, and 11.). Signal intensities from edematous regions after subtraction of noise as logarithmic functions of TI with least squares fits are presented in Figures 5, 6, and 7. The zero crossings for signal intensities calculated from the functions of least squares fits are presented in Table 6.

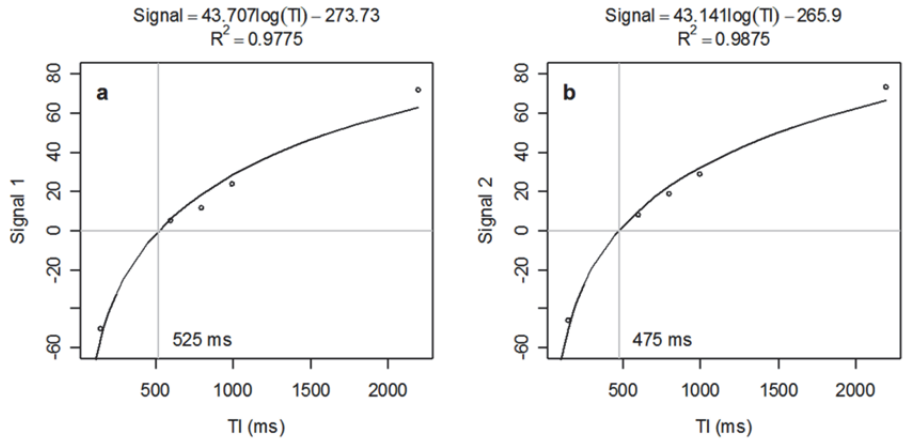

Fig. 5. Inversion time tests in patient case 1. Measured signal intensities (in arbitrary units) from two areas (a,b) inside edema with five inversion times (150, 600, 800, 1000, 2200) are indicated with circles. Logarithmic least square fits (solid line) were used to calculate zero-points for signal intensity (marked near TI axis).

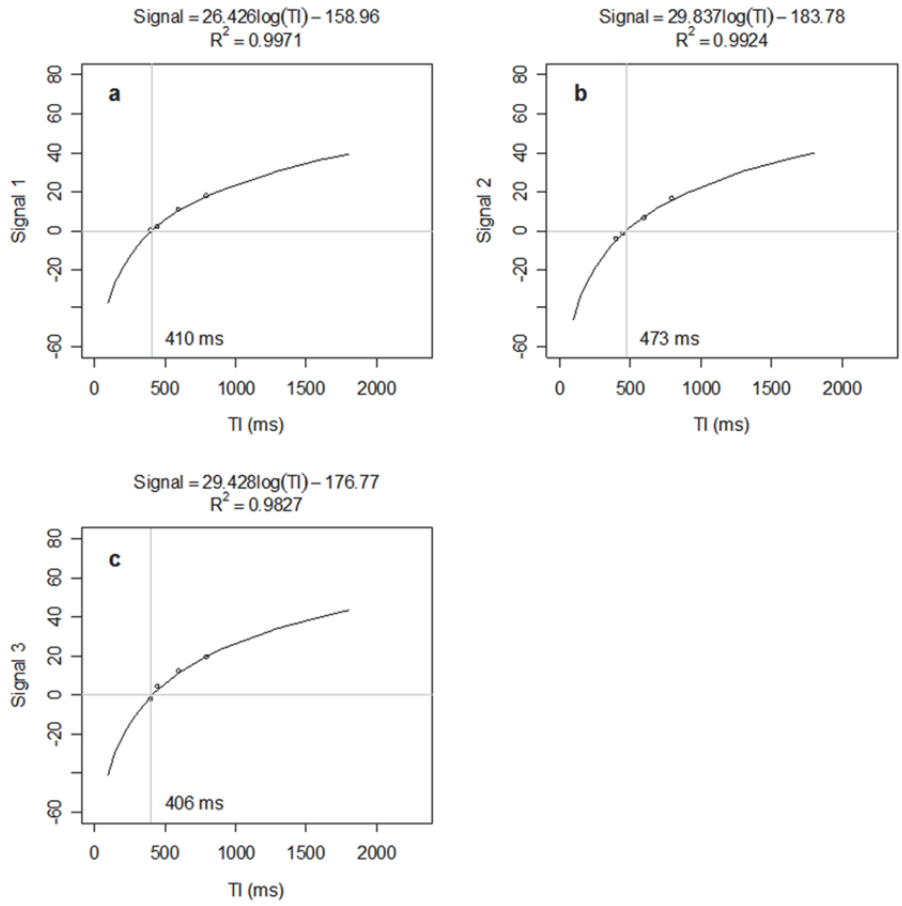

Fig. 6. Inversion time tests in patient case 2. Measured signal intensities (in arbitrary units) from three areas (a,b,c) inside edema with four inversion times (400, 448, 600, 800) are indicated with circles. Logarithmic least square fits (solid line) were used to calculate zero-points for signal intensity (marked near TI axis).

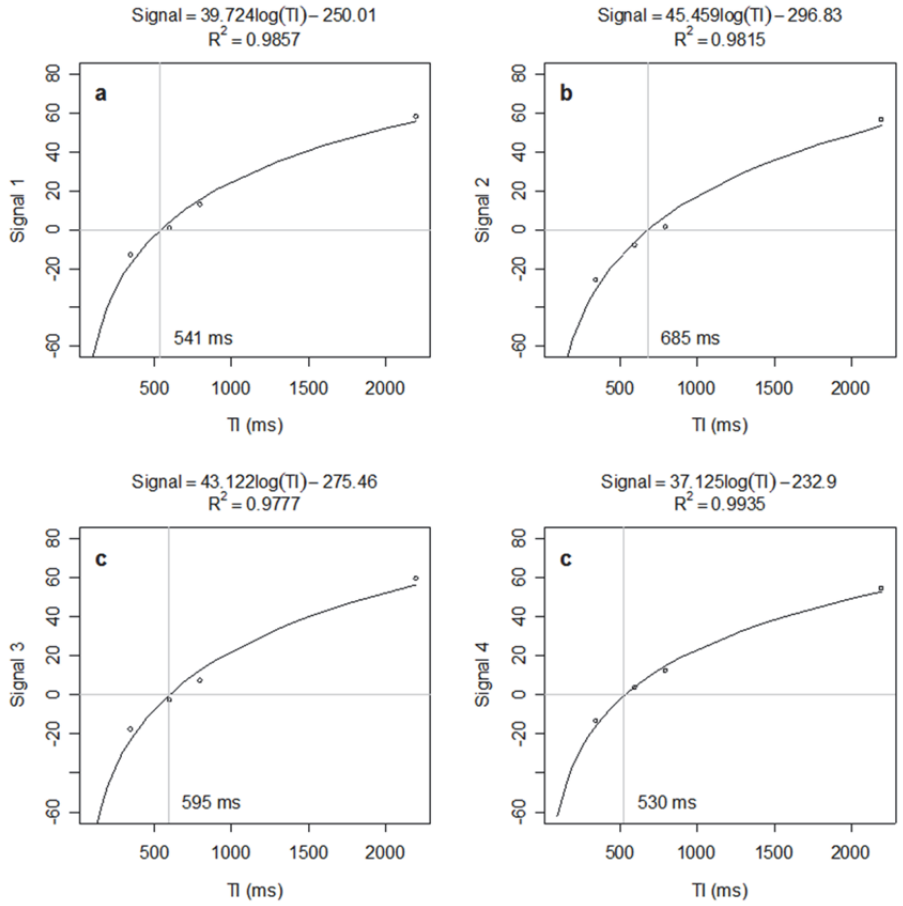

Fig. 7. Inversion time test in patient 3. Measured signal intensities (in arbitrary units) from four areas inside edema with four inversion times (350, 600, 800, 2200) indicated with circles. Logarithmic least square fits (solid line) are used to calculate zero-points for signal intensity (marked near TI axis).

Table 6. Calculated inversion time values for signal attenuation of edematous areas.

Patient	Area 1		Area 2		Area 3		Area 4	
	TI (ms)	T_1 (ms)	TI (ms)	T_1 (ms)	TI (ms)	T_1 (ms)	TI (ms)	T_1 (ms)
1	509	734	568	819				
2	410	592	477	688	406	586		
3	558	805	721	1040	618	892	546	788

TI, inversion time; T_1, relaxation time; ms, milliseconds

Tests for clinically feasible TI values were based on observations by neurosurgeons and neuroradiologists. Three patients were described as illustrative cases representing the different practical advantages of this sequence in surgical decision making. The results of the clinical usefulness and the main advantages of the IR pulse sequence for brain tumor surgery were:

- MRI signal from edema was suppressed with TI between 400 milliseconds and 800 milliseconds. In most cases, the best suppression was achieved with TI 600 milliseconds.
- Non-enhancing and scattered tumor volume was better delineated in EDAIR than on T_1- or T_2-weighted images.

Case 1

This 40-year-old previously healthy male presented with epileptic seizures. The epilepsy was caused by a right temporal lobe brain tumor with poorly defined borders on T_1- and T_2- weighted images. The maximal diameter of the tumor was more than 6 cm and it did not enhance with contrast medium. The tumor contained a cyst and showed an edema reaction within the surrounding brain tissue. The preoperative MRI study performed in the 0.23-T scanner included IR sequences with TIs of 2200, 1000, 800, 600, and 150. The main tumor mass was well defined with IR pulse sequences (Fig 8).

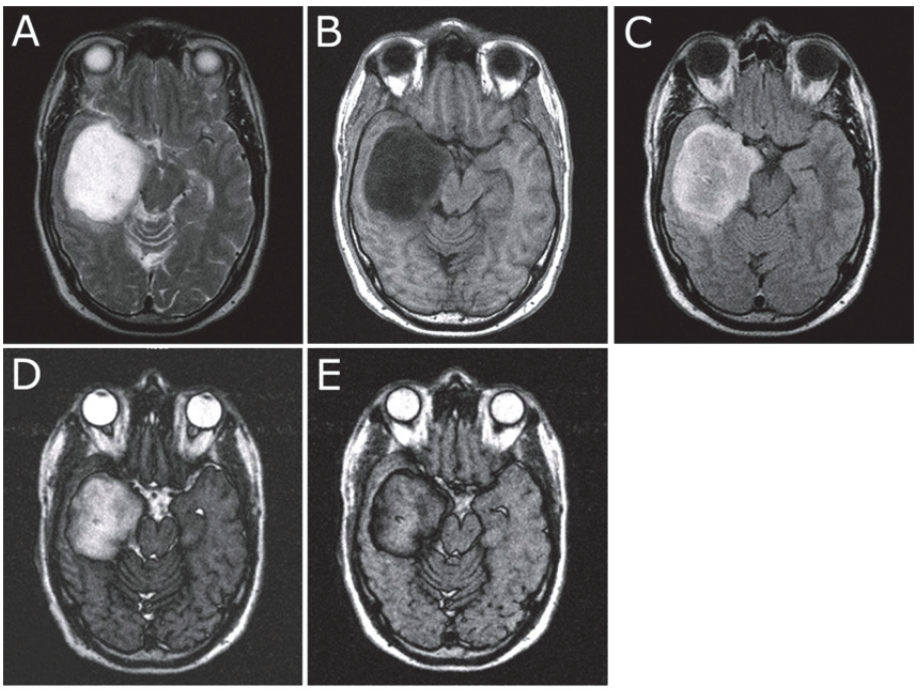

Fig. 8. (Case 1). A large cystic tumor is in the right temporal lobe (low-grade fibrillary astrocytoma, WHO grade II). T_2 (A) and T_1 (B) sequences show the tumor, but the delineation of the tumor is not clear. The inner structure of the tumor seems homogenous in both (A) and (B). FLAIR (C) shows the inner structure of the tumor better, but the IR sequence with TI of 600 ms (D) and TI of 800 ms (E) are the sequences that in addition make the margins of the tumor most visible.

The resection of the tumor was performed under intraoperative MRI guidance, and the IR sequence was used to assist radical resection of the tumor. There was a pseudocapsule at the anterior part of the tumor seen in edema suppression images. The posterior part grew infiltratively without any clear margin medially up from the free edge of the tentorium. In this region, the tumor boundaries were not sharply demarcated on the edema-suppressed images.

The postoperative MRI study included IR sequences with TI of 2200, 1000, 800, and 600. The latter images showed blood and cerebrospinal fluid in the resection cavity (Fig 9). The IR with TI 600 milliseconds sequence was scanned also after intravascular administration of contrast medium (Magnevist 15 mL). The intraoperative and postoperative MRI controls with IR pulse sequence showed some gross tumor residual that was difficult to surgically differentiate

from medial structures. There were no complications during the surgery, and the patient was neurologically intact postoperatively. The histological diagnosis was diffuse low-grade fibrillary astrocytoma (WHO grade II) correlating with the neuroradiologic diagnosis.

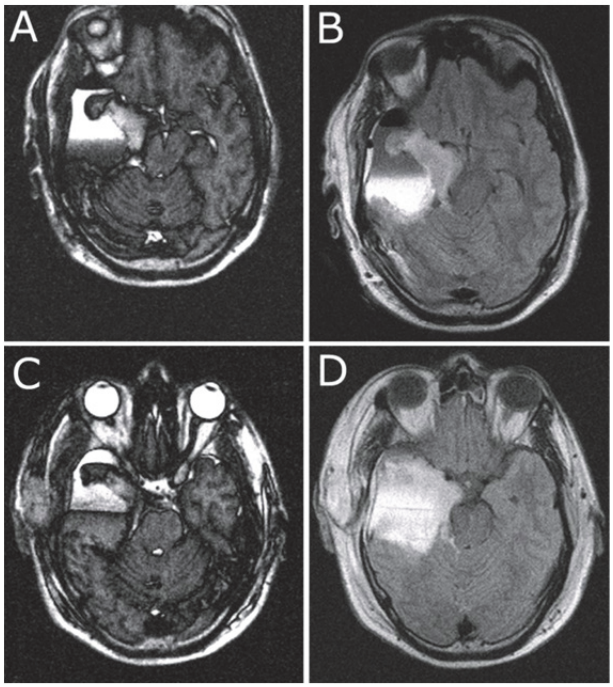

Fig. 9. Case 1 postoperatively. The resection cavity was filled with blood and cerebrospinal fluid that were separable with an inversion recovery sequence with inversion time of 600 ms (A) and 2200 ms (B) immediately after surgery. The same sequences were used 1 day later (C, D, respectively), indicating separable components in inversion recovery with inversion time 600 ms (C), but not with 2200 ms (D). Some residual tumor is evident medially.

Case 2

This 33-year-old female had been operated for a left frontal low-grade astrocytoma (WHO grade II) 6 years earlier. Postoperatively, she had received radiotherapy. A large, recurrent tumor with a maximal diameter of 5 cm was now

found on follow-up MRI. Clinically the patient suffered from moderate headache and epilepsy.

The recurrent tumor was growing expansively causing a 1-cm midline shift. It enhanced strongly with contrast medium. Preoperatively, an IR sequence with TI of 800 showed two different components in the tumor volume (Fig 10). These components were not separable on contrast enhanced T_1- and T_2-weighted MRI sequences. Craniotomy was performed and the solid enhancing tumor area was radically resected with intraoperative MRI guidance. Histological samples from both components of the tumor acquired under MR guidance showed a difference in the amount of collagen in the samples.

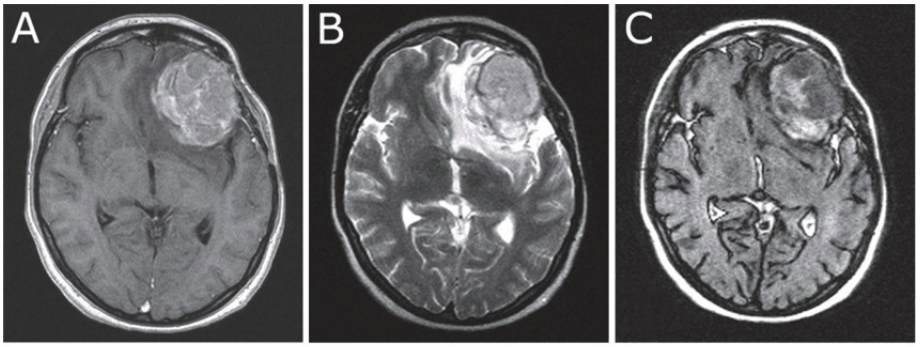

Fig. 10. Case 2. Inversion recovery (IR) sequence with TI of 800 milliseconds helps to delineate the tumor and visualize its inner structure. An enhancing tumor in the left frontal lobe is shown (malignant primitive neuroectodermal tumor [PNET]) in a contrast-enhanced T_1 magnetic resonance image (MRI) (A). With T_2-weighted MRI the edema is most evident but the delineation of the tumor from the edema is not clear (B). Using an IR sequence with a TI-weighted image of 800 milliseconds, the edema is suppressed. The tumor mass is well delineated, consisting of two different components in which a difference in the amount of collagen was detected later on histological examination of the tissue samples (C).

After surgery, the patient was neurologically intact. The postoperative MRI control showed no enhancing solid residual tumor in the surgical cavity. The edematous brain surrounding the surgical cavity was nonuniformly enhancing. The histology suggested a malignant primitive neuroectodermal tumor with features of neuroblastic and possibly also oligodendroglial differentiation.

Case 3

This 65-year-old, previously healthy male suffered from rapidly progressive left-sided hemiparesis and urinary incontinence. He also had one generalized epileptic seizure. MRI displayed two large tumors in the right frontal lobe. Preoperatively, the most likely diagnosis was glioblastoma multiforme. Open biopsy was performed under ultrasound and intraoperative MRI guidance.

Preoperative MRI included IR sequences with TIs of 2200, 800, 600, and 350. Sequences with TIs of 2200 and 600 were repeated after the intravascular infusion of contrast medium (Magnevist 15 mL). The edema suppressed images delineated the tumor better than did T_2, FLAIR, and T_1 images without contrast medium (Fig 11).

The histological diagnosis was glioblastoma multiforme (WHO grade IV). The patient was then referred for radiotherapy.

The tumor structure determined in the EDAIR images was essentially the same as that in contrast enhanced T_1 series. However, the contrast-enhanced EDAIR images were the most informative in estimating the tumor boundaries and the tumor soft-tissue contents. One by-product of this study was the superior visualization of the cerebral sulci, which can be used in dissection to achieve minimally invasive approaches to small subcortical tumors.

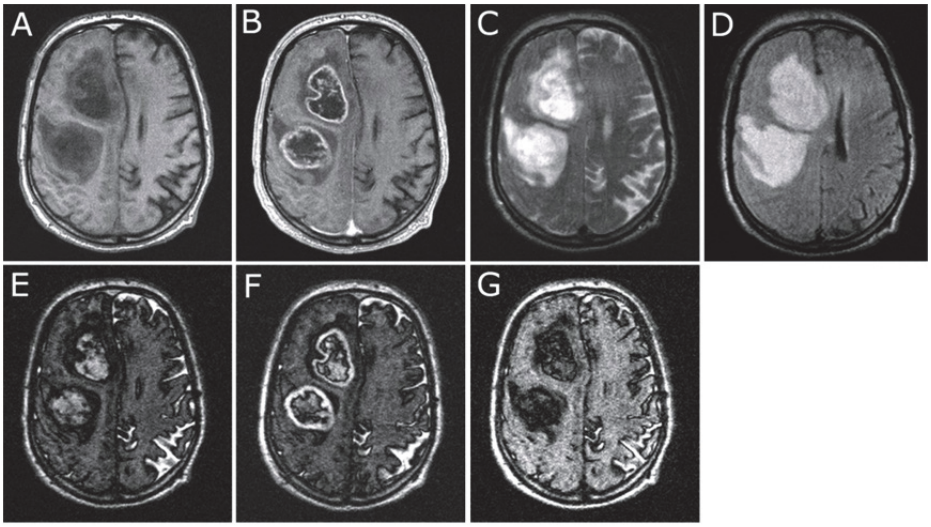

Fig. 11. (Case 3). IR sequence with TI of 600 ms without i.v. contrast medium could in this case show the delineation of tumors from the surrounding edema as well as did T_1 with contrast medium. Two large tumors in the right frontal lobe (glioblastoma multiforme, GBM) are shown in T_1 weighted sequences without (A) and with (B) contrast enhancement. The tumors are well delineated from the surrounding edema. In T_2 (C) and FLAIR (D) the edema is visible as high signal intensity, but the tumors cannot be demarcated. The IR sequence with TI of 600 ms both without (E) and with (F) contrast enhancement shows the delineation of the tumors from the edema. It should be noted that even in the non-enhanced IR TI 600 ms sequence the tumors are approximately of the same size as in the contrast enhanced T_1 sequence (B). The same TI cannot be applied to all patients, which is demonstrated when an IR sequence with TI of 800 ms was evaluated (G). In this case both the tumors and the edema were suppressed.

5.3 Neuronavigated ultrasound imaging in the intraoperative MRI environment

5.3.1 Interlink between ultrasound image and navigated MRI scan

The interlink between ultrasound image and the corresponding MRI scan plane was achieved with the customized instrument tracker (Fig 3B), which fulfilled the following clinical requirements: compatible with MRI scan, sterilizable,

ergonomic for surgical use, wide operating angle without loss of line-of-sight between IT and ir-camera, and tight fixation with one screw.

5.3.2 Correspondence measurements

Corresponding measurements with the US-MRI scan phantom showed spatial differences in all three compared pairs: MRI scan versus ultrasound image, MRI scan versus phantom, and ultrasound image versus phantom. In the case of the ultrasound image, the spatial difference increased as a function of distance from the ultrasound imaging probe. In MRI scans, the distance from the scanner's isocenter was the important factor causing spatial error. Qualitative imaging results are shown in Figure 12; the respective quantitative results are summarized in Table 7.

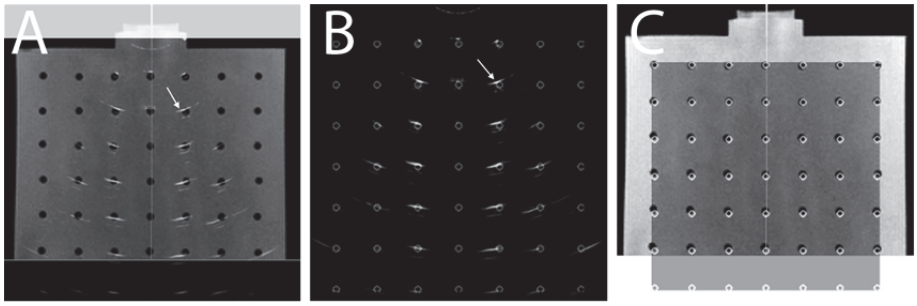

Fig. 12. Qualitative fusions between the MRI plane and the US image plane (A), the US image plane and the phantom rod matrix (B), and the MRI plane and the phantom rod matrix (C). (A) US echoes from the phantom's rods appeared as bright areas (arrow), whereas the rods in MR images were hypointense round areas. The correspondence between US and MR images was not exact. Deviation increased as a function of distance from the upper surface. (B) US echoes from the phantom's rods appeared as bright areas (arrow), whereas the rods in the phantom showed as white circles. Deviation of spatial information between US echoes and the real object was less than that between US and MRI. (C) The MR-image plane, where rods are hypointense, was reconstructed from the original 3D data set in the direction of the navigated US probe. The real locations of the rods appeared as white circles. There was spatial deviation in the MR images compared to the real spatial information. This deviation increased as a function of distance from the isocenter.

As can be seen in Table 7, quantitative spatial deviations between MRI scanning versus phantom and ultrasound image versus phantom were almost equal. However, the deviation in the MRI scanning versus ultrasound image was 45% larger because of summation of spatial deviation in opposite directions. Spatial error increased as a function of depth. Errors in both imaging modalities versus phantom increased only moderately as a function of depth. However, the relative error in ultrasound image versus MRI scanning increased to 4 mm at a depth of 100 mm. With one exception, the vertical deviations were substantially greater than the lateral deviations in all three compared pairs at all depths.

Table 7. Deviations of spatial information measured from image data at several depths.

Depth	Comparing pairs								
(mm)	MRI vs phantom			MRI vs US			US vs phantom		
	Δx (mm)	Δy (mm)	Σ (mm)	Δx (mm)	Δy (mm)	Σ (mm)	Δx (mm)	Δy (mm)	Σ (mm)
0–40	0.40	0.36	*0.57*	0.11	0.17	*0.21*	0.11	0.22	*0.29*
	±0.16	±0.09	*±0.20*	±0.15	±0.17	*±0.21*	±0.15	±0.30	*±0.29*
60–80	0.69	1.31	*1.55*	0.38	1.92	*1.98*	0.86	1.05	*1.41*
	±0.31	±0.36	*±0.37*	±0.24	±0.58	*±0.61*	±0.31	±0.26	*±0.25*
100–120	0.71	1.79	*1.95*	1.17	3.50	*3.74*	1.33	1.72	*2.38*
	±0.35	±0.37	*±0.46*	±0.61	±0.28	*±0.34*	±1.33	±0.52	*±1.05*
0–120	*0.60*	*1.15*	*1.36*	*0.53*	*1.87*	*1.98*	*0.77*	*1.00*	*1.37*
	±0.32	*±0.60*	*±0.59*	*±0.48*	*±1.23*	*±1.30*	*±0.74*	*±0.56*	*±0.80*

Δx: lateral deviation; Δy: vertical deviation; Σ: total deviation

5.3.3 Surgery with the present system

An awake craniotomy in the iMRI scan suite was performed. The patient's head was fixed to the head frame (adjustable in four directions). The head was kept in the same position. The dura was opened before iMRI scanning. After iMRI scanning, the scanner was shut down and the patient was moved outside the scanner; the distance from the scanner was approximately 1 m. At that position, the navigated IOUS was applied immediately after iMRI scanning (Fig 13) and several times during surgery. At operation, a distinct grayish tumor was noted protruding from the Sylvian fissure after opening the dura. Navigated IOUS showed a major part of the resectable tumor to be in the Sylvian fissure with crablike tumor extension over the insula. The insula was clearly less echogenic. The tumor was meticulously removed from the fissure. The underlying insula appeared healthy. Bipolar stimulation of the surgical field cortex revealed no

effect on speech (counting from 1 to 10) or on motor functions in the face or limbs. The resected tumor was an anaplastic oligodendroglioma, and biopsies taken from its border to the adjacent edematous frontal and temporal lobe showed some tumor infiltration. The patient made an uneventful recovery and was referred for radiation therapy.

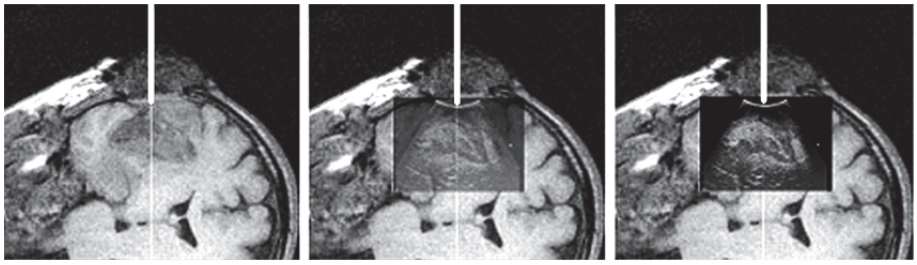

Fig. 13. The ultrasound image with 3 transparency levels 0, 50 and 100% was fused into the oblique MRI plane calculated with the neuronavigation software from the contrast-enhanced T_1-weighted 3D MRI scan data. The series of images shows how the tumor infiltration of the Sylvian fissure, corresponging to the surgical findings is more clearly revealed in the ultrasound image.

5.4 O-arm based stereotactic neurosurgery

5.4.1 Surgery with the present system

The patients in the validating series were 6 consecutive patients operated for various indications, since the O-arm assisted procedure itself required no new experimental actions. The O-arm study replaced the CT imaging that had been routinely used and merged with MR images.

The required MRI 3D-T_1-weighted and T_2-weighted datasets were scanned preoperatively a day before the operation and trajectory plans for the implantable instruments were made based on the MR-images with excellent soft tissue demarcation.

In the operating room, right after the Leksell stereotactic frame was fixed to the patient's head and the patient was positioned in a comfortable position on the operating table, the O-arm was used to collect a 3D dataset in the enhanced mode for calculation of the target coordinates. After scanning the O-arm was moved to its parked position. The surgical table and the head fixation concept worked well

and did not limit use of the O-arm. The patient's position could be optimally adjusted to assure comfort.

While the patient was prepped and draped, the surgeons and the physicist calculated the target coordinates. The 3D dataset was imported into the StealthViz software of the S7 navigation system. With the StealthViz software the patient specific O-arm dataset and the generic CT dataset from the coordinate calculation box without the patient were merged to become one single dataset. The new dataset was exported into the FrameLink stereotactic calculation software, which was able to recognize all nine rods on the plates and to formulate coordinates inside the brain. In FrameLink, MRI datasets were then merged to the O-arm dataset. Coordinates of the selected targets were calculated based on the rods in the O-arm images and anatomical information and plans on the MR-images. This phase including the 3D scanning and calculation, required approximately 15 minutes, which was much shorter than the time needed for a visit to the radiological department for MRI or CT.

The surgical operation was done as usual with O-arm control as needed. The automated positioning system helped to park the gantry of the O-arm away from the surgical area and then to drive it back over the patient's head when 2D or 3D images were needed, so the control images could be taken in seconds. The flat panel detector offered good quality wide area 2D images for control of localization of DBS, MER or thalamotomy electrodes. Image quality was good for intraoperative requirements and ensured exact location of the electrodes.

At the end of the operation a 3D dataset was scanned. It showed the exact locations of implanted electrodes. The dataset could be merged with the preoperative plan to compare the planned and the real locations of the DBS-electrodes.

5.4.2 Radiation doses

Patients were exposed to ionizing radiation during 2D and 3D O-arm scanning. The 2D fluoroimages with minor doses were mainly used for a fast check of the instrument trajectory and position in the brain and to verify the O-arm's optimal position for the 3D scan. Usually 4–10 fluoroimages were needed. High dose 3D-scans were required for the planning and calculation of coordinates at the beginning and for the control images at the end of the operation. Calculated radiation doses in the enhanced mode, which was used to achieve better soft tissue contrast, were 5 to 10 times higher than those in the standard mode. The

Finnish Radiation and Nuclear Safety Authority (Säteilyturvakeskus, STUK) has determined the maximum dose limits for a single CT-scan, which are 65 mGy (CTDI, computed tomography dose index) for the brain and 90 mGy (CTDI) for the skull. CTDI values for the O-arm shown in Table 8 were less than the 90 mGy limit for the skull and equivalent to the 65 mGy limit for the brain.

Table 8. Calculated radiation doses in 2D and 3D scanning modes in our patients.

Patient	2D			3D				
	Exp. time (s)	Exposure (mGy)	DAP (mGy*cm2)	Scannings	kVp	mAs	CTDI (mGy)	DLP (mGy*cm)
1	9.4	10.0	2247	2	100	596	53.8/107.7	1722
2	6.6	3.9	872	2	100	745	67.4/134.7	2154
3	6.8	6.3	1411	2	110	596	64.3/128.5	2056
4	11.9	7.9	1798	2	100	744	67.3/134.5	2154
5	3.6	2.8	621	2	100	596	53.8/107.7	1722
6	8.1	9.7	2175	2	110	595	64.2/128.4	2054

DAP, dose area product; kVp, peak kilovoltage; mAs, milliampere second; CTDI, computed tomography dose index; DLP, dose length product

5.4.3 Accuracy

The spatial accuracy of the images and technical accuracy of the concept were determined using two custom-made phantoms.

The spatial accuracy of images could be checked qualitatively from the images by comparing the known structure of the phantom to the locations of the structures on the images as shown in Figure 14. Materials in the stereotactic frame could decrease image quality due to artefacts, but artefacts did not influence spatial accuracy.

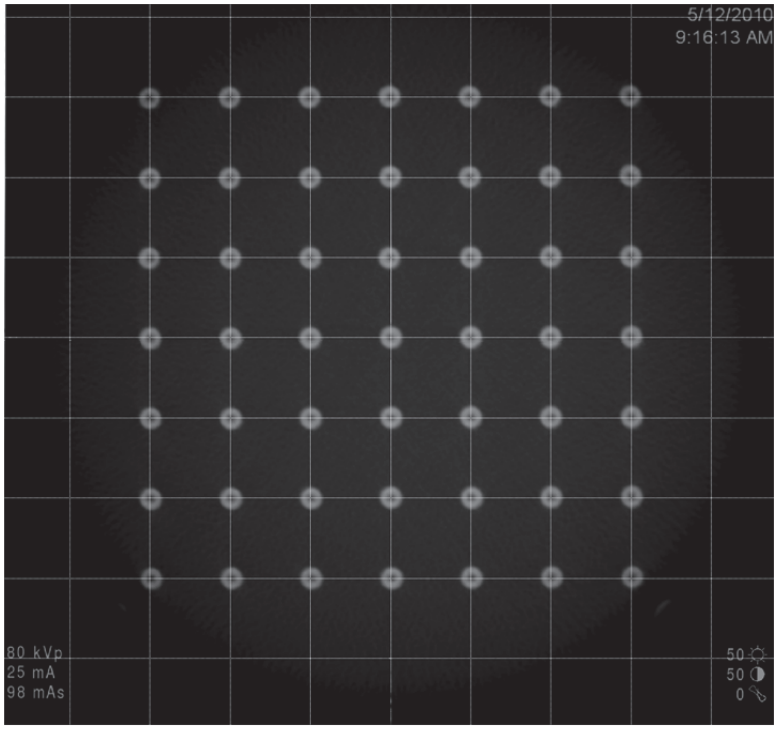

Fig. 14. In the O-arm image the rods (grey circles with black centers) of the spatial accuracy phantom were seen in correct positions within 22 mm separations from each other. The gray line grid was overlaid on the image to check correctness of the spatial information in the O-arm images. The spatial accuracy could thus be verified throughout the 3D volume.

The calculation accuracy of the concept was measured using the technical accuracy phantom with artificial STN targets scanned five times in different positions. From all five datasets the target coordinates of both STNs, left and right, were calculated as in the patient cases and the calculated coordinates of the targets were compared to the exact X, Y and Z values (Table 9, Fig 15).

Total displacement errors were 0.47 ± 0.07 mm on the left and 0.60 ± 0.16 mm on the right side. In the X, Y and Z directions displacements were respectively 0.18 ± 0.10 mm, 0.2 ± 0.08 mm and 0.3 ± 0.12 mm on the left side and 0.18 ± 0.10 mm, 0.32 ± 0.10 mm and 0.38 ± 0.26 mm on the right side. The concept's technical accuracy proved to be similar to the level of the voxel size of the O-arm images. The voxel size was 0.415 mm × 0.415 mm × 0.833 mm.

Table 9. The technical accuracy of the O-arm guided concept (values are in mm).

	Left							Right						
	X	|ΔX|	Y	|ΔY|	Z	|ΔZ|	TOT	X	|ΔX|	Y	|ΔY|	Z	|ΔZ|	TOT
REAL	112.0		97.0		114.0			88.0		97.0		114.0		
O1	112.0	0.0	96.8	0.2	114.5	0.5	0.54	88.0	0.0	96.6	0.4	114.9	0.9	0.98
O2	112.2	0.2	96.8	0.2	113.9	0.1	0.30	88.2	0.2	96.7	0.3	114.0	0.0	0.36
O3	112.3	0.3	97.4	0.4	113.8	0.2	0.54	88.3	0.3	97.1	0.1	113.5	0.5	0.59
O4	112.3	0.3	97.1	0.1	114.3	0.3	0.44	88.3	0.3	96.6	0.4	114.3	0.3	0.58
O5	111.9	0.1	96.9	0.1	113.6	0.4	0.42	87.9	0.1	96.6	0.4	113.8	0.2	0.46
AVER	112.14	0.18	97.00	0.20	114.02	0.30	0.45	88.14	0.18	96.72	0.32	114.10	0.38	0.60
SD	0.15	0.10	0.20	0.08	0.30	0.12	0.07	0.15	0.10	0.15	0.10	0.40	0.26	0.16

X, Y and Z, coordinates in the Leksell stereotactic system; |ΔX|, |ΔY| and |ΔZ|, absolute values of the displacement from the exact coordinates; TOT, total displacement calculated by the Pythagorean theorem; REAL, real coordinate values; O1, O2, O3, O4 and O5, different O-arm datasets; SD, standard deviation;

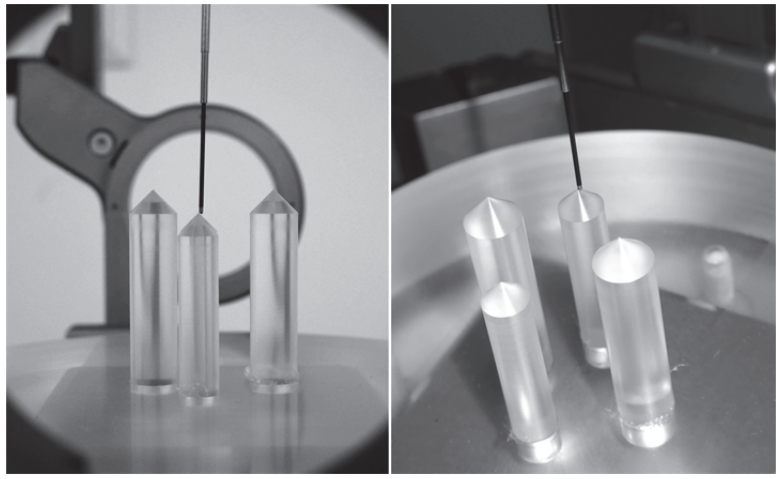

Fig. 15. A total displacement error of less than 0.5 mm can be seen mainly in the anterior direction, which falls within the size of the O-arm imaging voxel.

5.4.4 Intracerebral hemorrhage

In stereotactic DBS operations, intracerebral hemorrhage is a risk and must be excluded during or after the procedure. To study the application of O-arm imaging for detection of blood intracranially, two patients were scanned as part of their surgery for acute hematoma. One patient had an acute spontaneous ICH and the

other an acute subdural hematoma. Images showed clear demarcation of the ICH (Fig 16) and the SDH.

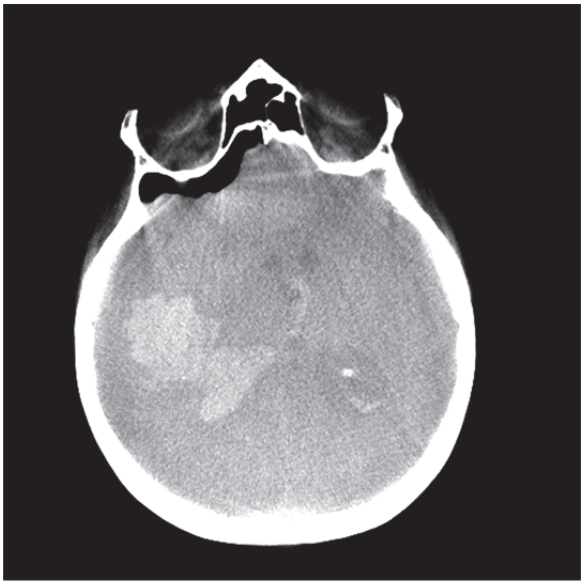

Fig. 16. This O-arm image was taken from a patient suffering from a spontaneous ICH, about four hours after bleeding, and placement of ventrical catheter. Image showing intracranial air (black areas in the frontal horns and subdurally) and remaining ICH (white areas).

6 Discussion

As stated in the introduction, the aim of brain surgery is to operate an intracranial object without surgery-related traumatization of healthy brain tissue. This intracranial object can be removable pathological tissue or a treatable functional target. Especially in tumor resections, according to the general principles of oncology, radical resection of brain tumors is expected to have a positive influence on the patients' prognosis both in terms of quality of life and progression-free survival time. There are some studies to support this statement in brain tumor surgery (Albert *et al.* 1994, Keles *et al.* 1999, Hall 2004).

From the history of imaging modalities it can be observed that development of medical imaging has notably influenced neurosurgery, i.e. better methods to determine the location and demarcation of the region of the surgical interest has been a key factor in safely reaching the functional target and in achieving radical resection (Kubben *et al.* 2011, Larson *et al.* 2011, Senft *et al.* 2011). Imaging modalities and navigation methods may increase accuracy of localization and delineation of the region of surgical interest. This has directly affected the patient's quality of life and life expectancy (McGirt *et al.* 2009, Sanai & Berger 2008, Stummer *et al.* 2006). Thus, multimodal imaging to collect information for preoperative planning and intraoperative guidance and control has been promoted.

It is also important to recognize from the recent century that we really are at the beginning of the history of image guidance. We are not at the final end in developing brain surgery. In the coming years there is a lot that can be done and learned to be better than today. Swedish neurosurgeon Lars Leksell has expressed: *"No technique could be too refined particularly with reference to the ability to localize and treat lesions in the brain"*.

6.1 Low-field intraoperative magnetic resonance imaging

The benefits of intraoperative MRI units for neurosurgical patients have been demonstrated and accepted widely (Black *et al.* 1997, Tronnier *et al.* 1997, Wirtz *et al.* 1997, Hall *et al.* 1998, Kollias *et al.* 1998, Martin *et al.* 1998, Steinmeier *et al.* 1998, Samset & Hirschberg 1999, Black *et al.* 1999, Hall *et al.* 1999, Seifert *et al.* 1999, Sutherland *et al.* 1999, Tyler & Mandybur 1999, Bernstein *et al.* 2000, Kaibara *et al.* 2000, Bohinski *et al.* 2001, Nimsky *et al.* 2001, Hadani *et al.* 2001, Levivier *et al.* 2003, Nimsky *et al.* 2003, Yrjänä 2003, Tuominen *et al.* 2003, Pamir *et al.* 2010). However, open discussion at the 3rd Meeting of the

Intraoperative Imaging Society in 2011 (IOIS, Zurich, Jan 16–19th) brought out unsolved questions. The most important are the questions: "What is the optimal, i.e. feasible and suitable, static magnetic field strength for intraoperative MRI?" and "Should the patient or the scanner be moved for the intraoperative scanning?".

In this thesis a concept based on a low-field scanner with a turn-off feature was designed for a combined imaging and operating room. The low field strength has been considered a drawback (Hall *et al.* 1999), because some imaging modalities, such as functional brain imaging and spectroscopy, are not possible intraoperatively. Some centers still agree that higher field strength is better (Nimsky *et al.* 2003). That is true from the radiological point of view, but still there are also surgical considerations that need to be addressed. The horizontally open resistive magnet enabled a staged imaging protocol during neurosurgical operations where, in our experience, there was usually no need for continuous imaging and intraoperative acquisition of functional data. Our solution offered the neurosurgeon adequate working space and reasonable ergonomics for operations that often last many hours.

Reliability, practicability and economic aspects still call for the use of some non-MRI-compatible instruments and devices in intraoperative MRI. Several centers with similar concepts seem to share this view (Tronnier *et al.* 1997, Steinmeier *et al.* 1998, Sutherland *et al.* 1999, Bernstein *et al.* 2000, Rubino *et al.* 2000). By turning off the magnetic field we were able to avoid safety risks associated with operating in the magnetic fringe field and we minimized the distance that the patient was moved between the imaging and surgical spaces to about 70 cm. Optically navigated localization of tumor remnants could be done routinely outside the imaging space to augment the staged operating and imaging practice.

The intraoperative low-field MRI unit provided a feasible possibility to control for brain shift and tumor remnants and to update the image data sets for the neuronavigator.

6.2 Edema suppression at low magnetic field strength

Tumor tissue is often surrounded by edema making it more difficult to determine surgically safe resectable regions. In the low magnetic field this difficulty may be more obvious than at high field strength (Hall *et al.* 1999, Nimsky *et al.* 2003). Thus edema attenuation was studied with inversion recovery MRI-sequences to suppress signal from edema and thereby help differentiate it from resectable

tumor and improve image quality in the low-field MRI unit. This was the first article on cerebral edema suppression with variable inversion times in a low magnetic field.

The explored EDAIR sequence gave valuable preoperative imaging data to delineate cerebral pathology. This information supplemented other imaging modalities, such as T_1- and T_2-weighted MRI sequences, and assisted the neurosurgeon in evaluating the region of surgical interest before craniotomy and in defining a safe trajectory to the tumor.

At 0.23 T magnetic field strength, the theoretically calculated TI for edema suppression was 451 milliseconds, varying from 348 milliseconds to 555 milliseconds with a standard deviation of 23% (Bottomley *et al.* 1987). Tests including three patients with four different TIs showed the feasible values as ranging from 406 milliseconds to 721 milliseconds. From the neurosurgical point of view, EDAIR images with TIs of 400–800 milliseconds were most valuable for image-guided procedures.

Both theoretical considerations and clinical tests showed that cerebral edema differed from patient to patient with respect to its T_1 relaxation time. An inversion time of approximately 400 milliseconds may suppress the edema in one patient, but may leave the area hyperintense in another. Thus the optimal TI for edema suppression varied from case to case. This same variation was reported to exist in the high magnetic field also (Lee *et al.* 2000). Based on this preliminary study, it seems that values of about 400 milliseconds could be too short for adequate suppression of edema and the signal to noise ratio of the images may be poor. However, the TI of 800 milliseconds did not suppress the edema signal in a region as large as at 600 milliseconds. TI 600 milliseconds gave an area of suppression comparable to the high intensity region on T_2-weighted images. These findings suggest that a TI of approximately 600 milliseconds could be optimal in most cases at 0.23 T.

There were also cases in which the EDAIR sequences suppressed approximately the region that was hyperintense in T_2-weighted images without distinction between tumor and edema. This might indicate that the tumor is highly infiltrative and intermingles with surrounding edematous brain tissue.

The hypointense boundary seen in some cases between apparent tumor bulk and surrounding tissue was due to the magnitude encoding of the magnetization. The signal from one side of the boundary had relaxed to a positive value at the time of data collection, whereas the other side was still negative. In magnitude encoding, both signals were shown in lighter tones than the boundary where

magnetization crossed zero. This feature could be used as one basis for defining the extent of resection. This phenomenon was seen especially when the chosen TI had not suppressed edema signal adequately or when edema had not been formed to a notable degree.

Based on our experience and the observations of other researchers, the leakage of intraoperatively used contrast medium might distort later intraoperative MRI sessions because of diffusion of contrast medium into the surrounding brain tissue around the operation cavity (Tronnier *et al.* 1997). All three illustrative cases shown in study II, especially case 3 (Fig 11), showed that an edema suppression sequence could be an option to replace intraoperative contrast enhanced T_1 sequences. However, the signal-to-noise ratio in our head frame coil restricted the use of some intraoperative edema suppression imaging times.

Edema suppression IR sequences in the low magnetic field could provide a valuable tool for preoperative planning of brain tumor resection. However, in clinical practice, economical and time constraints limit the acquisition of several sequences with different TIs as part of a routine protocol.

6.3 Optically navigated ultrasound imaging in the iMRI environment

In study III it was hypothesized that if two or more intraoperative imaging modalities were interlinked together with a neuronavigation method, the localization and the delineation of the region of surgical interest would be more reliable during the operation than with just one intraoperative imaging modality or with combined pre- and intraoperative modalities (Nabavi *et al.* 2001, Rasmussen *et al.* 2007). The illustrative case showed that intraoperative US can give valuable supplemental information to intraoperative MRI because it clearly showed the resectable tumor mass in the Sylvian fissure. Technically speaking, imaging modalities are based on simplified assumptions of physical phenomena which, nevertheless, might cause artifacts on images. For example, assumptions of homogenous static magnetic fields in MRI and of a constant speed for ultrasound waves in tissues in the intracranial volume are highly idealized. Thus, two independent imaging modalities based on different phenomena can supplement one another to reveal errors in spatial information (Rasmussen *et al.* 2007).

In most iMRI concepts using neuronavigation, the optical localization method, passive or active, is used (Kaibara *et al.* 2000, Hadani *et al.* 2001, Levivier *et al.* 2003). One benefit of optical localization is that the static and alternating electromagnetic fields in the MR-imaging environment do not disturb it. A disadvantage is the required line of sight between the instrument and the ir-cameras. Neurosurgeons freely used the ultrasound image probe within the line of sight to the ir-cameras because of the offset of the reflecting spheres from the probe. Even with a 90-degree angle, the ir-camera could see the sphere configuration. All materials were sterilizable and MRI-compatible. Rigidity of the materials and precision machining ensured tight fixation of the tracker to the ultrasound imaging transducer. Navigation of ultrasound imaging did not require repeated instrument length calibration because the construction was constant and the length had been defined in the transformation matrix.

The ultrasound/MRI-phantom developed in this study was suitable in both imaging modalities without causing artifacts. A phantom of this nature is not commercially available. The phantom seemed to be MRI-compatible because we could find no artifacts or distortions caused by magnetization or electrical currents. Thus, it was possible to determine deviations in spatial information in the ultrasound image and the MR-images with good accuracy. However, narrower polymethylmethacrylate rods might decrease the lateral spread of ultrasound echoes. A mild difference between the speed of ultrasound waves in the water filled phantom at room temperature and brain at body temperature might cause some error when analyzing real spatial accuracy of US. The speed of ultrasound in a water-filled phantom at room temperature and in living brain are 1480 m/s and 1562 m/s (Duck 1990), respectively. However, in US scanners the speed of ultrasound is simplified to be 1540 m/s. Speed variation as a function of frequency of ultrasound waves in soft tissues is thought to be insignificant (Kremkau *et al.* 1979, Kremkau *et al.* 1981, Duck 1990). However, the difference between speed (1480 m/s vs 1540 m/s) could cause spatial inaccuracy of a couple of millimeters.

Qualitative study of the deviation in spatial information showed clinically important information regarding the relative accuracy of these imaging modalities. Quantitatively, the average deviations of ultrasound image and MRI scanning compared with the true spatial data were 1.37 ± 0.80 mm and 1.36 ± 0.59 mm, respectively. Even more important was the vertical accuracy compared with the real phantom as a function of depth. Compared with the measured locations of the phantom rods, ultrasound images showed them to be deeper, whereas the

reconstructed MR-images showed them to be closer. In the fringe field of the phantom, MRI-scan deviation alternated randomly because of the inhomogeneity of the static field. The deviation between ultrasound image and MRI was remarkable in deep objects; at a depth of 100 to 120 mm, it was 3.74 ± 0.34 mm.

With one exception, vertical deviations were substantially greater than lateral deviations in all three compared pairs at all depths. However, the narrow sector of the present ultrasound imaging probe limited full observation in the lateral fringe area.

The clinical application of optical neuronavigation to combine iMRI and IOUS scanning with or without Doppler seems to be feasible. The use of a non-MRI-compatible ultrasound scanner in the present MRI scanning environment was possible because of the shutdown feature of the resistive static magnetic field, with a relatively short 6-minute ramp-up time. Shutdown allows transfer of the ultrasound scanner next to the MRI scanner. One minor limitation in the present navigation system was that ultrasound images and MRI scans were displayed on separate monitors.

In summary, according to this first of its kind study and the results of Rasmussen *et al.* (Rasmussen *et al.* 2007), optically neuronavigated ultrasound imaging together with iMRI scanning can provide valuable supplemental intraoperative information, both spatially and qualitatively. Our recommendation based on this unique report is to connect ultrasound imaging to iMRI scanning or at least to preoperative MR images. This imaging multimodality is most important in small and critical regions of surgical interest.

6.4 Intraoperative CT in frame-based stereotaxy

Study IV showed that the O-arm, an orthopedically optimized 3D-scanning system, could be used alone as an intraoperative imaging method during frame based stereotactic operations (Caire *et al.* 2010, Shahlaie *et al.* 2011, Smith & Bacay 2011). In this study, considered to be the first in the world, the O-arm could replace perioperative MR and CT imaging methods for the targeting. The concept proved to be accurate and straightforward and it shortened OR time.

According to the accuracy results, the concept itself – including merging two datasets to be a single one – did not decrease accuracy. The technical accuracy in the X-Y-plane was comparable to the pixel size. The X direction was the most accurate as it was determined directly from the pixels. The displacement in the Y direction was slightly less accurate as shown by inaccuracies in the determination

of the rods in the coordinate calculation box in the Y direction. In the Z direction the differences between calculated and real coordinates were largest, which can be explained by the slice thickness of 0.833 mm which is greater than the pixel size.

Radiation doses in the enhanced mode were higher than expected. The Finnish Radiation and Nuclear Safety Authority had limited the maximum dose levels to 65 mGy for brain per one CT scan and this level was exceeded in some cases. At least two data sets, preoperatively for the planning and postoperatively to ensure location of the DBS electrodes, should be obtained, which causes an overall dose of 130 mGy, if both scans are done in the enhanced mode for ventricle visualization and to rule out hemorrhage. Especially for younger patients undergoing stereotactic biopsy or DBS implantations for epilepsy, obsessive-compulsive disorder or dystonia, the dose levels need to be optimized.

Stereotactic operations through a burr hole are associated with a minor risk of bleeding (Binder *et al.* 2005). Based on our long term experience of intraoperative control monitoring, i.e. imaging and microelectrode recording, we assume that the risk of bleeding exists even if high quality angiography data is used during planning. The risk exists because of the brain shift caused by cerebrospinal fluid (CSF) leakage. If bleeding could be detected during operation, it might diminish the possibility of serious intracerebral hemorrhage. Intraoperative O-arm scanning at the end of the operation before closure could show bleeding at the acute phase, even without contrast enhancement.

More than just controlling the location of implanted electrodes, the O-arm can give unique and valuable information which cannot be achieved without intraoperative 3D scanning. The 3D data can be used to analyze intraoperative intracranial changes and possible errors in the overall implantation method. Sometimes postoperative scanning with MRI or CT can give the same information, but not with the same details and the spatial accuracy of real intraoperative scanning. Intraoperative data clearly reveals immediate brain shift due to the operation. Amounts and directions of the shifts can be analyzed to study the brain shift around the region of the surgical interest. This can be most valuable in epilepsy DBS-cases where the targets, the anterior thalamic nuclei, are below the lateral ventricles and can markedly shift with cerebrospinal fluid leakage (unpublished results). The 3D datasets can also be used to check how much the DBS electrodes have moved after the implantation.

6.5 Future views

Information obtained from intraoperative imaging methods is valuable for visualizing the surgical region of interest at any time, and can be used to control and guide the operation more accurately than with preoperative images alone. Also the use of two or more imaging modalities could reveal spatial inaccuracies and limitations in another scanning method which is used in parallel. For example, one physical phenomenon is capable of providing excellent soft tissue contrast while another is better at showing pulsating arteries in the same region.

It is recommended that modern neurosurgical centers apply image guided methods, at least neuronavigation, but also some intraoperative imaging methods which can be used to update navigation data. Highly sophisticated centers already utilize intraoperative MRI alone or with US. Some centers, in particular DBS-centers, should plan to have intraoperative CT. This is even more important because use of the MRI scanners for target calculations is limited in the future since new MRI scanners utilize smaller head coils to achieve increased SNR for better image quality. The size of the coils prevents scanning patients with a stereotactic frame. Therefore coordinate calculations have to be done with CT or a CT-like method such as the O-arm. Thus, in the future, stereotactic centers using frame based stereotactic methods and MR imaging based coordinate calculation could use the surgical O-arm in the operating room as an intraoperative scanning method instead of CT outside of the operating rooms.

In addition to the anatomical images of US, CT and MRI, it is recommended to utilize also other imaging modalities such as tractography, different functional data and biochemical information to get a better understanding of the region of surgical interest. However, this data could be collected preoperatively.

State of the art neurosurgical operating centers should have i) optical and electromagnetic navigation systems, ii) an easily and quickly applied low-field MRI unit, iii) a dedicated high-field 3 T MRI unit next to the OR, which can be employed at the beginning of the operation and during operation if time consuming high quality images are needed, iv) a navigated US system, v) a navigated microscope with optical fluorescence, vi) a movable intraoperative CT unit with angiography possibilities and vii) possibilities to apply tractography and other modern information and to modify this information during operation by the surgeons themselves.

7 Conclusions

1. The open, low-field MRI scanner as an intraoperative imaging tool may be useful especially in the context of neuronavigation. A scanner that can be turned off during surgery is particularly appropriate for neurosurgery.
2. At 0.23 T field strength, inversion recovery sequences with suitable inversion time supplement other imaging modalities and assist neurosurgeons in evaluating different surgical trajectories and in estimating brain tumor volume before craniotomy. An inversion time of approximately 600 milliseconds is optimal in most cases at 0.23 T. The effect of better distinction between edema and tumor tissue was most evident in cases which both suppression of edema and enhancement of tumor tissue with contrast agent were used.
3. Neurosurgeons can obtain valuable supplemental knowledge of the location and demarcation of brain tumors intraoperatively using the method of optically neuronavigated intraoperative US in an intraoperative MRI scanning environment. The method allows neurosurgeons to interlink two imaging modalities based on different physical phenomena. Furthermore, critical spatial image distortions can be observed when comparing the two modalities. Intraoperatively collected and interlinked images may enhance understanding of the region of surgical interest.
4. The O-arm can be utilized overall in stereotactic DBS operations from the calculation of the stereotactic target coordinates to final verification of the placement of the electrodes. It is possible to plan and verify trajectories by identifying normal landmark structures of the brain, to discover and correct intraoperatively any deviations between the planned and the real position of the instruments, and to exclude serious complications, especially intracerebral hematoma.
5. Overall, many different imaging modalities could be used in neurosurgery intraoperatively. Different physical phenomena reveal different aspects of the region of the surgical interest. Especially intraoperatively collected images and interlinked datasets may enhance understanding of the region of surgical interest.

References

Albert FK, Forsting M, Sartor K, Adams HP & Kunze S (1994) Early postoperative magnetic resonance imaging after resection of malignant glioma: objective evaluation of residual tumor and its influence on regrowth and prognosis. Neurosurgery 34: 45–61.

Alexander E III, Moriarty TM, Kikinis R & Jolesz FA (1995a) Innovations in minimalism: Intraoperative MRI. Clinical Neurosurgery 43: 338–352.

Alexander E III, Kooy HM, van Herk M, Schwartz M, Barnes PD, Tarbell N, Mulkern RV, Holupka EJ & Loeffler JS (1995b) Magnetic resonance image-directed stereotactic neurosurgery: use of image fusion with computerized tomography to enhance spatial accuracy. J Neurosurg 83: 271–276.

Barnett GH, Kormos DW, Steiner CP & Weisenberger J (1993a) Intraoperative localization using an armless, frameless stereotactic wand. J Neurosurg 78: 510–514.

Barnett GH, Kormos DW, Steiner CP & Weisenberger J (1993b) Use a frameless, armless stereotactic wand for brain tumor localization with two-dimensional and three-dimensional neuroimaging. Neurosurgery 33: 674–678.

Barnett GH, Kormos DW, Steiner CP, Piraino D, Weisenberger J, Hajjar F, Wood C & McNally J (1993c) Frameless stereotaxy using a sonic digitizing wand: development and adaptation to the Picker ViStar medical imaging system. In: Maciunas RJ (ed) Interactive Image-Guided Neurosurgery. Neurosurgical Topics, American Association of Neurological Surgeons: 113–119.

Beckmann EC (2006) CT scanning the early days. The British Journal of Radiology 79: 5–8.

Bernstein M, Al-Anazi AR, Kucharczyk W, Manninen P, Bronskill M & Henkelman M (2000) Brain tumor surgery with the Toronto open magnetic resonance imaging system: Preliminary results for 36 patients and analysis of advantages, disadvantages, and future prospects. Neurosurgery 46(4): 900–909.

Bhagwandien R (1994) Object induced geometry and intensity distortions in magnetic resonance imaging. Ph.D. thesis, University of Utrecht.

Binder DK, Rau GM & Starr PA (2005) Risk factors for hemorrhage during microelectrode-guided deep brain stimulator implantation for movement disorders. Neurosurgery 56: 722–732.

Bittar RG, Olivier A, Sadikot AF, Andermann F, Comeau RM, Cyr M, Peters TM & Reutens DC (1999) Localization of somatosensory function by using positron emission tomography scanning: a comparison with intraoperative cortical stimulation. J Neurosurg 90(3): 478–483.

Black PMcL, Moriarty T, Alexander E III, Stieg P, Woodard EJ, Gleason PL, Martin CH, Kikinis R, Schwartz RB & Jolesz F (1997) Development and implementation of intraoperative magnetic resonance imaging and its neurosurgical applications. Neurosurgery 41(4): 831–845.

Black PM, Alexander E III, Martin C, Moriarty T, Nabavi A, Wong TZ, Schwartz RB, Jolesz F (1999) Craniotomy for tumor treatment in an intraoperative magnetic resonance imaging unit. Neurosurgery 45: 423–433.

Black M, Jolesz FA & Medani K (2011) From vision to reality: the origins if intraoperative MR imaging. Acta Neurochirurgica Supplementum 109: 3–8.

Bohinski RJ, Kokkino AK, Warnick RE, Gaskill-Shipley MF, Kormos DW, Lukin RR & Tew JM Jr (2001) Glioma resection in a shared-resource magnetic resonance operating room after optimal image-guided frameless stereotactic resection. Neurosurgery 48(4): 731–742.

Bottomley PA, Hardy CJ, Argersinger RE & Allen-Moore G (1987) A review of 1H nuclear magnetic resonance relaxation in pathology: are T1 and T2 diagnostic? Med Phys 14: 1–37.

Braun V, Dempf S, Tomczak R, Wunderlich A, Weller R & Richter HP (2001) Multimodal cranial neuronavigation: direct integration of functional magnetic resonance imaging and positron emission tomography data: technical note. Neurosurgery 48(5): 1178–1181.

Brommeland T & Hennig R (2000) Mechanical accuracy of a new stereotactic guide. Acta Neurochir 142: 449–454.

Caire F, Gantois C, Torny F, Ranoux D, Maubon A, Moreau JJ (2010) Intraoperative use of the Medtronic O-arm for deep brain stimulation procedures. Stereotact Funct Neurosurg 88: 109–114

Chandler WF, Knake JE, McGillicuddy JE, Lillehei KO & Silver TM (1982) Intraoperative use of real-time ultrasonography in neurosurgery. J Neurosurgery 57: 157–163.

Chandler WF & Rubin JM (1986) Intraoperative use of real-time ultrasound in neurosurgery. Contemp Neurosurg 8: 1–7.

Coenen VA, Mädler B, Schiffbauer H, Urbach H, Allert N (2011) Individual fiber anatomy of the subthalamic region revealed with DTI - A concept to identify the DBS target for tremor suppression Neurosurgery 68(4): 1069–1075.

Dorward NL, Alberti O, Velani B, Gerritsen FA, Harkness WFJ, Kitchen ND & Thomas DGT (1999) Postimaging brain distortion: magnitude, correlates and impact on neuronavigation. Neurosurg Focus 6(3).

Duck FA (1990) Physical properties of tissue, A comprehensive reference book. Academic Press: 73–135.

Düssik KT (1942) Uber die möglichkeit, hoch frequente mechaniche Schwingungen als diagnostisches Hilfsmittel zu verwerten. Z ges Neurol Phychiat 174: 153–168.

Edwards PJ, Hawkes DJ, Penney GP & Clarkson MJ (2001) Guiding Therapeutic Procedures. In: Hajnal JV, Hill DL G & Hawkes DJ (eds) Medical Image Registration, Chapter 12. CRC Press.

Engle DJ & Lunsford LD (1987) Brain tumor resection guided by intraoperative computed tomography. Journal of Neuro-Oncology 4: 361–370.

Evans AC, Peters TM, Collins DL, Neelin P & Gabe C (1993) Image registration based on discrete anatomic structures. In: Maciunas RJ (ed) Interactive Image Guided Neurosurgery. Neurosurgical Topics, American Association of Neurosurgical Surgeons: 17–43.

Fenster A & Downey DB (1996) 3-D ultrasound imaging: A review. IEEE Engineering in Medicine and Biology 15(6): 41–51.

Ferrant M, Nabavi A, Macq B, Black PM, Jolesz FA, Kikinis R & Warfield SK (2002) Serial registration of intraoperative MR images of the brain. Medical Image Analysis 6: 337–359.

French LA, Wild JT & Neal D (1950) Detection of cerebral tumors by ultrasonic pulses. Pilot studies on postmortem material. Cancer 3: 705–708.

French LA, Wild JT & Neal D (1951) The experimental application of ultrasonics to the localization of brain tumors. J Neurosurg 8: 198–203.

Gamache Jr FW (1997) The EasyGuide Neuro Image-Guided Surgery System. Neurosurgery 40(5): 1092–1096.

Ganslandt O, Steinmeier R, Kober H, Vieth J, Kassubek J, Romstock J, Strauss C & Fahlbusch R (1997) Magnetic source imaging combined with image-guided frameless stereotaxy: a new method in surgery around the motor strip. Neurosurgery 41(3): 621–627.

Germano IM, Villalobos H, Silvers A & Post KD (1999) Clinical use of the optical digitizer for intracranial neuronavigation. Neurosurgery 45(2): 261–270.

Gooding GAW, Edwards MSB, Rabkin AE & Powers SK (1983) Intraoperative real-time ultrasound in the localization of intracranial neoplasms. Radiology 146: 459–462.

Grode ML & Komaiko MS (1983) The role of intraoperative ultrasound in neurosurgery. Neurosurgery 12(6): 624–628.

Gronningsaeter A, Unsgård G, Ommedal S & Angelsen BAJ (1996) Ultrasound-guided neurosurgery: A feasibility study in the 3–30 MHz frequency range. British Journal of Neurosurgery 10(2): 161–168.

Gronningsaeter A, Kleven A, Ommendal S, Aarseth TE, Lie T, Lindseth F, Lango T & Unsgård (2000) SonoWand, an ultrasound-based neuronavigation system. Neurosurgery 47(6): 1373–1380.

Gumprecht H & Lumenta CB (2003) Intraoperative imaging using a mobile computed tomography scanner. Minim Invasive Neurosurg 46: 317–322.

Hadani M, Spiegelman R, Feldman Z, Berkenstadt H, Ram Z (2001) Novel, compact, intraoperative magnetic resonance imaging-guided system for conventional neurosurgical operating rooms. Neurosurgery 48(4): 799–807.

Hall WA, Martin AJ, Liu H, Pozza CH, Casey SO, Michel E, Nussbaum ES, Maxwell RE & Truwit CL (1998) High-field strength interventional magnetic resonance imaging for pediatric surgery. Pediatr Neurosurg 29: 253–259.

Hall WA, Martin AJ, Liu H, Nussbaum ES, Maxwell RE & Truwit CL (1999) Brain biopsy using high-field strenght interventional magnetic resonance imaging. Neurosurgery 44(4): 807–814.

Hall WA, Liu H, Martin AJ, Pozza CH, Maxwell RE, Truwit CL (2000) Safety, efficacy, and functionality of high-field strength interventional magnetic resonance imaging for neurosurgery. Neurosurgery 46(3): 632–642.

Hall WA, Liu H, Maxwell RE & Truwit CL (2003) Influence of 1.5-Tesla intraoperative MR imaging on surgical decision making. Acta Neurochir Suppl 85: 29–37.

Hall WA (2004) Extending survival in gliomas: surgical resection or immunotherapy. Surg Neurol 61: 145–148.

Hammoud MA, Ligon BL, ElSouki R, Shi WM, Schomer DF & Sawaya R (1996) Use of intraoperative ultrasound for localizing tumors and determining the extent of resection a comprative study with magnetic resonance imaging. J Neurosurg 84: 737–741.

Hatiboglu MA, Weinberg JS, Suki D, Rao G, Prabhu SS, Shah K, Jackson E & Sawaya R (2009) Impact of intraoperative high-field magnetic resonance imaging guidance on glioma surgery: a prospective volumetric analysis. Neurosurgery 64: 1073–1081.

Henderson JM, Smith KR & Bucholz RD (1994) An accurate and ergonomic method of registration for image-guided neurosurgery. Comput Med Imaging Graph 18(4): 273–277.

Hill CR (1973) Medical Ultrasonics: an historical review. British Journal of Radiology 46: 899–905.

Hirschberg H, Samset E, Hol PK, Tillung T, Lote K (2005) Impact of intraoperative MRI on the surgical results for high-grade gliomas. Minim Invasive Neurosurg 48: 77–84.

Hogan RE, Lowea VL & Bucholza RD (1999) Triple-Technique (MR Imaging, Single-Photon Emission CT, and CT) Coregistration for Image-Guided Surgical Evaluation of Patients with Intractable Epilepsy. American Journal of Neuroradiology 20: 1054–1058.

Hosoda T, Takeuchi H, Hashimoto N, Kitai R, Arishima H, Kodera T, Higashino Y, Sato K, Kikuta K (2011) Usefulness of intraoperative computed tomography in surgery for low-grade gliomas: a comparative study between two series without and with intraoperative computed tomography. Neurol Med Chir 51: 490–5.

Jakola AS, Unsgård G & Solheim O (2011) Quality of life in patients with intracranial gliomas: the impact of modern image-guided surgery. J Neurosurg 114(6): 1622–1630.

Jolesz FA (1994) MRI-guided interventions. GE Medical Systems, The Coolidge Scientific Review: 2.

Jolesz FA & Blumenfeld SM (1994) Interventional use of magnetic resonance imaging. Magnetic Resonance Quarterly 10(2): 85–96.

Judy PF (1995) Computed tomography: Reconstruction principles. In: Bronzino JD (ed) The Biomedical Engineering Handbook. CRC Press: 1002–1005.

Kaibara T, Saunders JK & Sutherland GR (2000) Advances in mobile intraoperative magnetic resonance imaging. Neurosurgery 47(1): 131–138.

Kato A, Yoshimine T, Hayakawa T, Tomita Y, Ikeda T, Mitomo M, Harada K, Mogami H (1991) A frameless, armless navigational system for computer-assisted neurosurgery. Technical note. J Neurosurg 74(5): 845–849.

Kaus M, Steinmeier R, Sporer T, Ganslandt O & Fahlbusch R (1997) Technical accuracy of a neuronavigation system measured with a high-precision mechanical micromanipulator. Neurosurgery 41(6): 1431–1437.

Kavic MS (1995) Three-dimensional ultrasound. Surgical Endoscopy 10: 74–76.

Keles GE, Anderson B & Berger MS (1999) The effect of extent of resection on time to tumor progression and survival in patients with glioblastoma multiforme of the cerebral hemisphere. Surg Neurol 52: 371–379.

Kiuru A (1985) Lääketieteelliset kuvausmenetelmät: fysiikka ja tekniikka. Turku, Gamma: 81–90.

Knake JE, Bowerman RA, Silver TM & McCracken S (1985) Neurosurgical applications of intraoperative ultrasound. Radiologic Clinics of North America 23(1): 73–90.

Koivukangas J (1984) Ultrasound imaging in operative neurosurgery: An experimental and clinical study with special reference to ultrasound holographic B (UHB) imaging. Acta Univ Oul D 115.

Koivukangas J, Louhisalmi Y, Alakuijala J & Oikarinen J (1993a) Ultrasound-controlled neuronavigator-guided brain surgery. J Neurosurg 79: 36–42.

Koivukangas J, Louhisalmi Y, Alakuijala J, Oikarinen J (1993b) Neuronavigator-guided cerebral biopsy. Acta Neurochir Suppl 58: 71–74.

Koivukangas J, Katisko J, Yrjänä S, Tuominen J, Schiffbauer H & Ilkko E (2003) Successful neurosurgical 0.23T intraoperative MRI in a shared facility. Proceedings of the 12th European Congress of Neurosurgery (EANS). Bologna, Italy: Monduzzi Editore Medimond: 439–444.

Koivukangas T, Katisko J & Koivukangas J (2011) Technical Accuracy Assessment of the Optical Tracking System of Surgical Navigators (submitted).

Koivula A (2002) Magnetic resonance image distortions due to artificial macroscopic objects. Ph.D. thesis, University of Oulu, Department of Diagnostic Radiology.

Kollias SS, Bernays R, Marugg RA, Romanowski B, Yonekawa Y & Valavanis A (1998) Target definition and trajectory optimization for interactive MR-guided biopsies of brain tumors in an open configuration MRI system. J Magn Reson Imaging 8(1): 143–159.

Kossoff G, Griffiths KA & Kadi AP (1995) Transducer rotation: A Useful scanning maneuver in three-dimensional ultrasonic volume imaging. Radiology 195: 870–872.

Kremkau FW, McGraw CP & Barnes (1979) Acoustic properties of normal and abnormal human brain. In Linzer M (ed) Ultrasonic Tissue Characterization II. National Bureau of Standards Spec Publ 525: 81–84.

Kremkau FM, McGraw CP & Barnes (1981) Ultrasonic attenuation and propagation speed in normal human brain. J Acoust Soc Am 70: 29–38.

Krings T, Buchbinder BR, Butler WE, Chiappa KH, Jiang HJ, Rosen BR & Cosgrove GR (1997) Stereotactic Transcranial Magnetic Stimulation: Correlation with Direct Electrical Cortical Stimulation. Neurosurgery 41: 1319–1326.

Kubben PL, ter Meulen KJ, Schijns OE, ter Laak-Poort MP, van Overbeeke JJ & van Santbrink H (2011) Intraoperative MRI-guided resection of glioblastoma multiforme: a systematic review. Lancet Oncol 12(11): 1062–1070.

Kuo JS, Yu C, Petrovich Z & Apuzzo ML (2003) The CyberKnife Stereotactic Radiosurgery System: Description, Installation, and an Initial Evaluation of Use and Functionality. Neurosurgery 53(5): 1235–1239.

Lango T (2000) Ultrasound guided surgery: image processing and navigation. Ph.D. thesis, NTNU Trondheim. ITK-rapport 2000: 12-W.

Larson PS, Starr PA, Bates G, Tansey L, Richardson RM & Martin AJ (2011) An Optimized System for Interventional MRI Guided Stereotactic Surgery: Preliminary Evaluation of Targeting Accuracy. Neurosurgery Jul 25.

Lauterbur PC (1973) Image formation by induced local interactions: examples employing nuclear magnetic resonance. Nature 242: 190–191.

Lee JK, Choi HY, Lee SW, Baek SY & Kim HY (2000) Usefulness of T1-weighted image with fast inversion recovery technique in intracranial lesions Comparison with T1-weighted spin echo image. J Clin Imaging 24: 263–269.

Leksell L (1956) Echo-encephalography. I. Detection of intracranial complications following head injury. Acta Chir Scand 110: 301–15.

Lewis JT, Galloway Jr. RL & Schreiner S (1998) An ultrasonic approach to localization of fiducial markers for interactive, image-guided neurosurgery – part 1: principles. IEEE Transactions on Biomedical Engineering 45(5): 620–630.

Levivier M, Wikler D, De Witte O, Van de Steene A, Baleriaux D & Brotchi J (2003) PoleStar N-10 low-field compact intraoperative magnetic resonance imaging system with mobile radiofrequency shielding. Neurosurgery 53(4): 1001–1006.

Lindstrom PA (1954) Prefrontal ultrasonic irradiation-a substitute for lobotomy. AMA Arch Neurol Psychiatry 72(4): 399–425.

Louw DF, Fielding T, McBeth PB, Gregoris D, Newhook P & Sutherland GR (2004) Surgical robotics: a review and neurosurgical prototype development. Neurosurgery 54(3): 525–536.

Lunsford LD, Leksell L, Jernberg B (1983) Probe holder for stereotactic surgery in the CT scanner. A technical note. Acta Neurochir 69: 297–304.

Manwaring KH (1993) Intraoperative microendoscopy. In: Maciunas RJ (ed) Interactive Image-Guided Neurosurgery. Neurosurgical Topics, American Association of Neurological Surgeons: 217–232.

Manwaring KH, Manwaring ML & Moss SD (1994) Magnetic field guided endoscopic dissection through a burr hole may avoid more invasive craniotomies, a preliminary report. Acta Neurochir (suppl) 61: 34–39.

Marmula R, Hilbert M & Niederdellmann H (1998) Intraoperative precision of mechanical, electromagnetic, infrared and laser-guided navigation systems in a computer-assisted surgery. Mun Kiefer Gesichtschir 2 (suppl) 1: 145–148.

Martin AJ, van Vaals JJ, Hall WA, Liu H & Truwit CL (1998) Intra-operative MR monitoring in neurosurgery. MedicalMundi 42(2): 12–21.

Mascott CR (2005) Comparison of magnetic tracking and optical tracking by simultaneous use of two independent frameless stereotactic systems. Neurosurgery 57(4 Suppl): 295–301.

Masuzawa H, Kamitani H, Sato J, Inoya H, Hachiya J & Sakai F (1981) Intraoperative application of sector scanning electronic ultrasound in neurosurgery. Neurol Med Chir 21(3): 277–285.

Matula C, Rössler K, Reddy M, Schindler E & Koos WT (1998) Intraoperative computed tomography guided neuronavigation: concepts, efficiency, and work flow. Comput Aided Surg 3: 174–182.

Maurer Jr. CR & Fitzpatrick JM (1993) A review of medical image registration. In: Maciunas RJ (ed) Interactive Image Guided Neurosurgery. Neurosurgical Topics, American Association of Neurosurgical Surgeons: 17–43.

Maurer Jr. CR, Fitzpatrick JM, Wang MY, Galloway RL, Maciunas RJ & Allen GS (1997) Registration of head volume image using implantable fiducials markers. IEEE Transactions on Medical Imaging 16(4): 447–462.

Maurer CR Jr, Hill DL, Martin AJ, Liu H, McCue M, Rueckert D, Lloret D, Hall WA, Maxwell RE, Hawkes DJ & Truwit CL (1998) Investigation of intraoperative brain deformation using a 1.5-T interventional MR system: preliminary results. IEEE Trans Med Imaging 17(5): 817–825.

Mayfrank L, Bertalanffy H, Spetzger U, Klein HM & Gilsbach JM (1994) Ultrasound-guided crationomy for minimally invasive exposure of cerebral convexity lesions. Acta Neurochirurgica 131: 270–273.

McGirt MJ, Chaichana KL, Gathinji M, Attenello FJ, Than K, Olivi A, Weingart JD, Brem H & Quiñones-Hinojosa AR (2009) Independent association of extent of resection with survival in patients with malignant brain astrocytoma. J Neurosurg 110(1): 156–162.

McInerney J & Roberts DW (2000) Frameless stereotaxy of the brain. The Mount Sinai Journal of Medicine 67: 300–310.

Nabavi A, Black PM, Gering DT, Westin CF, Mehta V, Pergolizzi RS Jr, Ferrant M, Warfield SK, Hata N, Schwartz RB, Wells WM 3rd, Kikinis R & Jolesz FA (2001) Serial intraoperative magnetic resonance imaging of brain shift. Neurosurgery 48(4): 787–797.

Nimsky C, Ganslandt O, Cerny S, Hastreiter P, Greiner G & Fahlbusch R (2000) Quantification of, visualization of, and compensation for brain shift using intraoperative magnetic resonance imaging. Neurosurgery 47(5): 1070–1079.

Nimsky C, Ganslandt O, Kober H, Buchfelder M & Fahlbusch R (2001) Intraoperative magnetic resonance imaging combined with neuronavigation: a new concept. Neurosurgery 48(5): 1082–1091.

Nimsky C, Ganslandt O, von Keller B & Fahlbusch R (2003) Preliminary experience in glioma surgery with intraoperative high-field MRI. Acta Neurochir Suppl 88: 21–29.

Nimsky C (2011) Intraoperative MRI in glioma surgery: proof of benefit? Lancet Oncol 12(11): 982–983.

Nixon MA, McCallum BC, Fright WR & Price NB (1998) The Effects of Metals and Interfering Fields on Electromagnetic Trackers. Presence 7(2): 204–218.

Ohye C, Kawashima Y, Hirato M, Wada H, Nakajima H (1984) Stereotactic CT scan applied to stereotactic thalamotomy and biopsy. Acta Neurochir 71: 55–68.

Oikarinen J, Alakuijala J, Louhisalmi Y, Sallinen S, Helminen H & Koivukangas J (1993) The Oulu Neuronavigator System: Intaoperative ultrasonography in the verification of neurosurgical localization and visualization. In: Maciunas RJ (ed) Interactive Image Guided Neurosurgery. Neurosurgical Topics, American Association of Neurosurgical Surgeons: 233–246.

Ojala R, Vahala E, Karppinen J, Klemola R, Blanco-Sequeiros R, Vaara T & Tervonen O (2000) Nerve root infiltration of the first sacral root in MRI guidance. JMRI 12: 556–556.

Pamir MN, Ozduman K, Dinçer A, Yildiz E, Peker S & Ozek MM (2010) First intraoperative, shared-resource, ultrahigh-field 3-Tesla magnetic resonance imaging system and its application in low-grade glioma resection. J Neurosurg 112: 57–69.

Parizel PMRJ (1994) The influence of field strenght on magnetic resonance imaging: a comparative study in physiochemical phantoms, isolated brain specimens and clinical applications. Antwerpen, Universitaire Instelling Antwerpen.

Pennec X, Ayache N, Roche A & Cachier P (2001) Non-rigid MR/US registration for tracking brain deformations. IEEE Computer Society Press (ed) Proc of Int. Workshop on Medical Imaging and Augmented Reality (MIAR 2001), Shatin, Hong Kong: 79–86.

Quencer RM & Montalvo BM (1986) Intraoperative cranial sonography. Neuroradiology 28: 528–550.

Raabe A, Krishnan R, Wolff R, Hermann E, Zimmermann M & Seifert V (2002) Laser surface scanning for patient registration in intracranial image-guided surgery. Neurosurgery 50(4): 797–801.

Rasmussen IA Jr, Lindseth F, Rygh OM, Berntsen EM, Selbekk T, Xu J, Nagelhus Hernes TA, Harg E, Håberg A & Unsgaard G (2007) Functional neuronavigation combined with intra-operative 3D ultrasound: initial experiences during surgical resections close to eloquent brain areas and future directions in automatic brain shift compensation of preoperative data. Acta Neurochir (Wien) 149(4): 365–378.

Redfern RM (1993) Historical perspective. In: Thomas DGT (ed) Stereotactic and Image Directed Surgery of Brain Tumours. London: Churchill Livingstone: 1–28.

Roberts DW, Strohbehn JW, Hatch JF, Murray W & Kettenberger H (1986) A frameless stereotaxic integration of computerized tomographic imaging and the operating microscope. J Neurosurg 65(4): 545–549.

Roberts DW, Hartov A, Kennedy FE, Miga MI & Paulsen KD (1998) Intraoperative brain shift and deformation: a quantitative analysis of cortical displacement in 28 cases. Neurosurgery 43(4): 749–760.

Roche A, Pennec X, Malandain G & Ayache N (2001) Rigid registration of 3-D ultrasound with MR images: a new approach combining intensity and gradient information. IEEE Transactions on Medical Imaging 20(10): 1038–1049.

Roux FE, Ibarrola D, Tremoulet M, Lazorthes Y, Henry P, Sol JC & Berry I (2001) Methodological and technical issues for integrating functional magnetic resonance imaging data in a neuronavigational system. Neurosurgery 49(5): 1145–1156.

Rubin JM & Dohrmann GJ (1983) Intraoperative neurosurgical ultrasound in the localization and characterization of intracranial masses. Radiology 148: 519–524.
Rubin JM & Dohrmann GJ (1985) Efficacy of intraoperative US for evaluating intracranial masses. Radiology 157: 509–511.
Rubin JM & Chandler WF (1990) Ultrasound in neurosurgery. New York, Raven Press: 70–106.
Rubino GJ, Farahani K, Mcgill D, Van De Wiele B, Villablanca JP & Wang-Mathieson A (2000) Magnetic resonance imaging-guided neurosurgery in the magnetic fringe fields: The next step in neuronavigation. Neurosurgery 46(3): 643–654.
Rumboldt Z, Huda W & All JW (2009) Review of portable CT with assessment of a dedicated head CT scanner. Am J Neuroradiol 30: 1630–1636.
Samset E & Hirschberg H (1999) Neuronavigation in intraoperative MRI. Comput Aided Surg 4(4): 200–207.
Sanai N & Berger MS (2008) Glioma extent of resection and its impact on patient outcome. Neurosurgery 62(4): 753–764.
Schenck JF, Jolesz FA, Roemer PB, Cline HE, Lorensen WE, Kikinis R, Silverman SG, Hardy CJ, Barber WD, Laskaris ET ym. (1995) Superconducting open-configuration MR imaging system for image-guided therapy. Radiology 195: 805–814.
Schenck JF (1996) The role of magnetic susceptibility in magnetic resonance imaging: MRI magnetic compatibility of the first and second kinds. Med Phys 23(6): 815–848.
Schiffbauer H (1999) Neuronavigation in Brain Tumor Surgery: Clinical Beta-phase of the Oulu Neuronavigator System. Acta Univ Oul D 505.
Schlaier J, Warnat J & Brawanski A (2002) Registration accuracy and practicability of laser-directed surface matching. Computer Aided Surgery 7: 284–290.
Seifert V, Zimmermann M, Trantakis C, Vitzthum H-E, Kühnel K, Raabe A, Bootz F, Schneider J-P, Schmidt F & Dietrich J (1999) Open MRI-guided neurosurgery. Acta Neurochir 141: 455–464.
Senft C, Franz K, Ulrich CT, Bink A, Szelényi A, Gasser T & Seifert V (2010) Low field intraoperative MRI-guided surgery of gliomas: a single center experience. Clin Neurol Neurosurg 112: 237–43.
Senft C, Bink A, Franz K, Vatter H, Gasser T & Seifert V (2011) Intraoperative MRI guidance and extent of resection in glioma surgery: a randomised, controlled trial. Lancet Oncol 12(11): 997–1003.
Shahlaie K, Larson PS & Starr PA (2011) Intraoperative Computed Tomography for Deep Brain Stimulation Surgery: Technique and Accuracy Assessment. Neurosurgery 68: ons114-ons124.
Shalit MN, Israeli Y, Matz S, Cohen ML (1979) Intra-operative computerized axial tomography. Surg Neurol 11: 382–384.
Shamir RR, Joskowicz L, Spektor S & Shoshan Y (2009) Localization and registration accuracy in image guided neurosurgery: a clinical study. Int J Comput Assist Radiol Surg 4(1): 45–52.

Shamir RR, Joskowicz L, Spektor S & Shoshan Y (2011) Target and trajectory clinical application accuracy in neuronavigation. Neurosurgery 68(1 Suppl, Operative): 95–102.

Smith AP & Bakay RA (2011) Frameless deep brain stimulation using intraoperative O-arm technology. J Neurosurg Apr 15.

Smith H-J & Ranallo FN (1989) A non-mathematical approach to basic MRI. Madison Wisconsin, Medical Physics Publishing Corporation.

Son BC, Kim MC, Choi BG, Kim EN, Baik HM, Choe BY, Naruse S & Kang JK (2001) Proton magnetic resonance chemical shift imaging (1H CSI)-directed stereotactic biopsy. Acta Neurochir 143(1): 45–49.

Steinmeier R, Fahlbusch, Ganslandt O, Nimsky C, Buchfelder M, Kaus M, Heigl T, Lenz G, Kuth R & Huk W (1998) Intraoperative magnetic resonance imaging with the magnetom open scanner: concepts neurosurgical indications, and procedures: a preliminary report. Neurosurgery 43(4): 739–748.

Steinmeier R, Rachinger J, Kaus M, Ganslandt O, Huk W & Fahlbusch R (2000) Factors influencing the apllication accuracy of neuronavigation system. Stereotact Funct Neurosurg 75(4): 188–202.

Stummer W, Stocker S, Wagner S, Stepp H, Fritsch C, Goetz C, Goetz AE, Kiefmann R & Reulen HJ (1998) Intraoperative Detection of Malignant Gliomas by 5-Aminolevulinic Acid-induced Porphyrin Fluorescence. Neurosurgery 42: 518–526.

Stummer W, Pichlmeier U, Meinel T, Wiestler OD, Zanella F & Reulen HJ (2006) Fluorescence-guided surgery with 5-aminolevulinic acid for resection of malignant glioma: a randomised controlled multicentre phase III trial. Lancet Oncol 7(5): 392–401.

Suess O, Kombos Th, Kurth R, Suess S, Mularski S, Hammersen S & Brock M (2001) Intracranial Image-Guided Neurosurgery: Experience with a new Electromagnetic Navigation System. Acta Neurochir 143: 927–934.

Sutcliffe JF (1991) Review article: The value of intraoperative ultrasound in neurosurgery. British Journal of Neurosurgery 5: 169–178.

Sutherland GR, Kaibara T, Louw D, Hoult DI, Tomanek B & Saunders J (1999) A mobile high-field magnetic resonance system for neurosurgery. J Neurosurg 91: 804–813.

Talos I-F, O'Donnell L, Westin C-F, Warfield SK, Wells III W, Yoo S-S, Panych LP, Golby A, Mamata H, Maier SS, Ratiu P, Guttmann CRG, Black PM, Jolesz FA & Kikinis R. (2003) Diffusion tensor and functional MRI fusion with anatomical MRI for image-guided neurosurgery. In: Ellis RE & Peters TM (eds) MICCAI 2003, LNCS 2878: 407–415.

Tronnier VM, Wirtz CR, Knauth M, Lenz G, Pastyr O, Bonsanto MM, Albert FK, Kuth R, Stauber A, Schlegen W, Sartor K & Kunze S (1997) Intraoperative diagnostic and interventional magnetic resonance imaging in neurosurgery. Neurosurgery 40(5): 891–902.

Truwit CL & Hall WA (2006) Intraoperative magnetic resonance imaging-guided neurosurgery at 3-T. Neurosurgery 58: ONS-338–45.

Tuominen J, Yrjänä SK, Katisko JP, Heikkilä J & Koivukangas J (2003) Intraoperative imaging in a comprehensive neuronavigation environment for minimally invasive brain tumour surgery. Acta Neurochir Suppl 85: 115–20.

Tyler D & Mandybur G (1999) Interventional MRI-guided stereotactic aspiration of acute/subacute intracerebral hematomas. Stereotact Funct Neurosurg 72: 129–135.

Unsgaard G, Ommendal S, Muller T, Gronninsaeter A & Nernes TAN (2002) Neuronavigation by intraoperative three-dimensional ultrasound: initial experience during brain tumor resection. Neurosurgery 50(4): 804–812.

Unsgaard G, Rygh OM, Selbekk T, Müller TB, Kolstad F, Lindseth F & Hernes TA (2006) Intra-operative 3D ultrasound in neurosurgery. Acta Neurochir 148(3): 235–253.

Vahala E, Ylihautala M, Tuominen J, Shiffbauer H, Katisko J, Yrjänä S, Vaara T, Ehnholm G & Koivukangas J (2001) Registration in Interventional Procedures With Optical Navigator. JMRI 13: 93–98.

Vahala E (2002) Methods for Interventional Magnetic Resonance Imaging. Helsinki University of Technology, Applied Electronics Laboratory, Series E: Electronic Publications E1. URI: http://lib.tkk.fi/Diss/2002/isbn9512261324/isbn9512261324.pdf. Cited 2011/03/30.

Watanabe E (1993) The neuronavigator: a potentiometer-based localizing arm system. In: Maciunas RJ (ed) Interactive Image-Guided Neurosurgery. Neurosurgical Topics, American Association of Neurological Surgeons: 135–147.

Wells PNT (1978a) History. In: deVlieger M, Holmes J, Kazner E, Kossof G, Kratochwil A, Kraus R, Poujol J & Strandness DE (eds) Handbook of Clinical Ultrasound. New York, John Wiley & Sons.

Wells PNT (1978b) Basic physics. In: deVlieger M, Holmes J, Kazner E, Kossof G, Kratochwil A, Kraus R, Poujol J & Strandness DE (eds) Handbook of Clinical Ultrasound. New York, John Wiley & Sons.

Wild JJ & Reid JM (1953) The effects of biological tissues on 15-mc pulsed ultrasound. J Acoust Soc Am 25(2): 270–280.

Wiles AD, Thompson DG & Frantz DD (2004) Accuracy assessment and interpretation for optical tracking systems. In: Galloway R (ed) Medical Imaging, Visualization, Image-Guided Procedures, and Display. Proc SPIE 5367: 421–432.

Wirtz CR, Bonsanto MM, Knauth M, Tronnier VM, Albert FK, Staubert A & Kunze S (1997) Intraoperative magnetic resonance imaging to update interactive navigation in neurosurgery: method and preliminary experience. Computer Aided Surgery 2: 172–179.

Woerdeman PA, Willems PW, Noordmans HJ, Tulleken CA & van der Sprenkel JW (2008) Application accuracy in frameless image-guided neurosurgery: a comparison study of three patient-to-image registration methods. J Neurosurg 106: 1012–1016.

Voorhies RM & Patterson RH (1980) Preliminary experience with intraoperative ultrasonographic localization of brain tumors. Radiol / Nucl Med Mag 10: 8–9.

Yamasaki T, Moritake K, Takaya M, Kagawa T, Nagai H, Akiyama Y & Kawahara M (1994) Intraoperative use of doppler ultrasound and endoscopic monitoring in the stereotactic biopsy of malignant brain tumors. J Neurosurg 80: 570–574.

Yrjänä S (2005) Implementation of 0.23 T magnetic resonance scanner to perioperative imaging in neurosurgery. Acta Univ Oul D 860.

Yu C, Apuzzo ML, Zee CS & Petrovich Z (2001) A phantom study of the geometric accuracy of computed tomographic and magnetic resonance imaging stereotactic localization with the Leksell stereotactic system. Neurosurgery 48(5): 1092–9.

Zaaror M, Bejerano Y, Weinfeld Z & Ben-Haim S (2001) Novel magnetic technology for intraoperative intracranial frameless navigation: in vivo and in vitro results. Neurosurgery 48(5): 1100–1108.

Original articles

I Yrjänä S, Katisko J, Ojala R, Tervonen O & Koivukangas J (2002) Versatile intraoperative MRI in neurosurgery and radiology. Acta Neurochir (Wien) 144: 271–278.

II Katisko J, Yrjänä S, Tuominen J, Kokkonen SM, Ilkko E, Erkkilä J, Shiffbauer H & Koivukangas J (2006) Cerebral edema attenuated inversion recovery MR sequence in low magnetic field: a feasibility study. Acad Radiol 13(2): 219–228.

III Katisko J & Koivukangas J (2007) Optically neuronavigated ultrasonography in an intraoperative magnetic resonance imaging environment. Neurosurgery 60(4 Suppl 2): 373–381.

IV Katisko J, Kauppinen M, Koivukangas J & Heikkinen E (2011) Stereotactic operations using the O-ARM. Manuscript.

Original publications are not included in the electronic version of the dissertation.

Book orders:
Granum: Virtual book store
http://granum.uta.fi/granum/

UNIVERSITY OF OULU P.O.B. 7500 FI-90014 UNIVERSITY OF OULU FINLAND

ACTA UNIVERSITATIS OULUENSIS

ISBN 978-951-42-9750-2 (Paperback)
ISBN 978-951-42-9751-9 (PDF)
ISSN 0355-3221 (Print)
ISSN 1796-2234 (Online)

UNIVERSITY of OULU
OULUN YLIOPISTO